https://doi.org/10.5194/egusphere-2024-2737
Preprint. Discussion started: 19 September 2024

Are rivers becoming more intermittent in France? Learning from an extended set of climate projections based on the Coupled Model Intercomparison Project phase 5 (CMIP5)

Tristan Jaouen[1], Lionel Benoit[2], Louis Héraut[1], Eric Sauquet[1]

[1]INRAE Lyon-Grenoble Auvergne-Rhône-Alpes, RiverLy, Villeurbanne, France
[2]INRAE PACA, Biostatistique et processus SPatiaux, Avignon, France

Correspondence to: Tristan Jaouen (tristan.jaouen@inrae.fr) and Eric Sauquet (eric.sauquet@inrae.fr)

Abstract

This study aims to assess the changes in the intermittency of river flows across France in the context of climate change. Projection of flow intermittence are derived from the results of the Explore2 project, which is the latest national study that proposes a wide range of potential hydrological futures for the 21st century. The multi-model approach developed within the Explore2 project enable to characterize uncertainties in future flow intermittence. Combined with discrete observations of flow states, hydrological projections are post-processed to compute the daily probability of flow intermittency (*PFI*) on each element of the partition of France in hydroecoregions (HER2).

The post-processing consists of calibrating logistic regressions between the historical flow states of the Observatoire National des Étiages (ONDE) network and the flow data simulated by the hydrological models (HMs) involved in Explore2 projected with the Safran reanalysis as inputs. After calibration, these regressions are used to project daily *PFIs* for the whole of the 21st century, based on flow simulations from five HMs driven by up to 17 climate projections under RCP 2.6, 4.5, and 8.5 climate change scenarios.

The results show good agreement among the HMs regarding the increase in flow intermittency under RCP 4.5 and 8.5. The changes in mean daily *PFI* between July and October, and the shifts in the first and last days when *PFI* exceeds 20%, suggest a gradual intensification and extension of dry spells throughout the century. The southern regions of France are likely to experience greater increases in runoff intermittency than the northern regions. Uncertainty is greater in northern France, due to the variability of rainfall. Mountainous regions such as the Alps and the Pyrenees are likely to experience changes in the dynamics of snowmelt and groundwater recharge, which could lead to changes in their runoff regimes.

1 Introduction

Intermittent Rivers and Ephemeral Streams (IRES) are watercourses characterized by the absence of continuous year-round water flow (Sefton et al., 2019). Flow intermittence results from various factors such as limited rainfall or freezing conditions,

https://doi.org/10.5194/egusphere-2024-2737
Preprint. Discussion started: 19 September 2024

or human-induced alterations of the runoff pattern. Climate is a primary driver of streamflow patterns, though geology and topography can also play significant roles in their development. Climate change is expected to modify the water cycle, with a significant reduction in summer precipitation and an increase in frequency of the heat waves in Western Europe (Vicente-Serrano et al., 2020), which is likely to result in more severe low flow periods and more frequent and widespread dry periods (Delso et al., 2017). Several features of flow intermittence such as its seasonality, duration, and spatial extent are likely to be altered, and a shift from perennial to intermittent flow may also affect many rivers (Van Meerveld et al., 2020). IRES play a central role as an interface between terrestrial and aquatic ecosystems. As a result, altered patterns of flow interruption can compromise water quantity and quality in downstream perennial rivers, endanger their specific biodiversity, and disrupt organic matter, nutrient, and sediment cycles, etc. (Meyer et al., 2007; Finn et al., 2011; Clarke et al., 2008; Gallart et al., 2012; Sarremejane et al., 2017). A better understanding of the behaviour of IRES and their interaction with perennial streams is therefore necessary to assess the impact of ongoing and future changes on river ecosystems (Döll and Schmied, 2012; Jaeger et al., 2014; Pumo et al., 2016; Leigh and Datry, 2017), and to address water management challenges (Acuña et al., 2014). Note that most past studies addressed the impact of climate change on flow intermittence at the local scale (e.g. in southern Italy, cf. (De Girolamo et al., 2022)) so there is a need to place these results in a wider context and to determine the extent of the changes and their consequences for the main rivers downstream.

To update the knowledge about the impact of climate change on water resources throughout its territory, France has recently implemented the project Explore2 (https://entrepot.recherche.data.gouv.fr/dataverse/explore2; Sauquet et al., in prep.). Through a multi-model and multi-scenario approach, Explore2 encompasses a wide range of possible hydrological futures for the whole 21st century, and therefore allows assessing the uncertainties arising at each step of the modelling process. However, the spatial resolution of the climate projections involved in Explore2 is too coarse to properly resolve IRES, in particular because IRES are usually small streams located in headwater catchments. To overcome this limitation and gain insight into IRES behaviour under climate change, the present study aims to extend the results of Explore2 to obtain projections of flow intermittence in headwater streams. We follow a statistical approach using streamflow data from large and perennial rivers to predict the daily Probability of Flow Intermittence (*PFI*). The *PFI* is defined as the proportion of headwater streams under drying conditions at a regional scale and is used as a proxy indicator for the intensity and duration of dry periods. Usually obtained in small watersheds (Sefton et al., 2019), it is calibrated using field campaigns specific to France, carried out regularly at more than 3200 upstream river sites prone to drying.

This approach has been initially developed and validated by Beaufort et al. (2018) using daily discharge and monthly flow intermittence observations over the period 2011-2017. Subsequently, this approach was leveraged by Sauquet et al. (2021) to project the *PFI* in a changing climate, but the spatial resolution of this "proof-of-concept" study was coarse and only a handful of climate scenarios were considered. The present study continues the enhancement on this *PFI* modelling framework, and in particular aims to increase the spatial resolution of future *PFI* projections, to consider a larger number of hydrological and

https://doi.org/10.5194/egusphere-2024-2737
Preprint. Discussion started: 19 September 2024

climate projections (thanks to Explore2 datasets), and to carefully quantify the uncertainties associated with the projected changes in river flow intermittence over the 21st century across France.

The paper is organized in five parts. The data used are outlined in the second section. The statistical method linking *PFI* to hydrological projections is described in Section 3, with results presented in Section 4. The results will focus on the mean daily *PFI* between July and October ($mPFI_{7\text{-}10}$), and the median of the first and last days (respectively, *Tf* and *Tl*) with *PFI* exceeded 20%. Finally Section 5 discusses these results, and Section 6 concludes the study.

2 Data

2.1 Monitoring river flow intermittence

The French Biodiversity Office (OFB, https://ofb.gouv.fr/) initiated the National Low-Flow Observatory (ONDE) in 2012 to gain a better understanding of low flows and intermittent rivers. ONDE is a stream intermittence monitoring network comprising 3248 observation sites strategically distributed across the French river network with the aim of characterizing the occurrence and the intensity of summer (low-) flows (Nowak and Durozoi, 2012). The network has been designed to focus on streams with a Strahler orders ranging from 1 to 4, which are prone to natural and/or anthropogenic intermittent flow conditions. Most sites (85%) are located on streams with a drainage area ≤ 100 km^2 and 20% of the sites have a drainage area ≤ 10 km^2.

A key feature of the ONDE network is that it involves the flow state of watercourses, which results from the visual inspection of streams by OFB observers at each location, instead of a sensor-based measurement of flow rates. In the present study, two binary categories are defined for ONDE observations: (1) "visible flows" and (2) "dry conditions", which gather non-visible flows (standing water in isolated pools) and totally dry conditions (dry riverbed at or near the ONDE site). The ONDE sites used in this study are monitored during field campaigns carried out systematically in mainland France around the 25th day of each month from May to September. We consider data from 2012 to 2022, and use these data for model calibration and evaluation. To ensure that the drying probability computed for each HER2 is not biased, ONDE field campaigns are only taken into account if at least 75% of the ONDE sites within a given HER2 are actually monitored during the campaign at hand.

2.2 Delineating areas with homogeneous hydrological behaviour: the Hydro-EcoRegions

Hydro-EcoRegions (HER) are spatially homogeneous areas defined over France based on natural drivers involved in river ecosystem functioning, such as geology, topography, and climate. There are 85 level-2 HER (HER2) across France, and they are derived from the sub-divisions of the 22 level-1 HER (HER1) (Wasson et al., 2002) which were used in the previous study about the impact of climate change on *PFI* in France (Sauquet et al., 2021). In contrast, the present study investigates flow intermittence at the scale of HER2 regions in order to model *PFI* at a higher spatial resolution. The statistical approach developed hereafter requires observations of flow states for calibration purposes (see Section 2.1.3) which led us to perform

https://doi.org/10.5194/egusphere-2024-2737
Preprint. Discussion started: 19 September 2024

five groupings of HER2 in order to ensure that enough observations are available for model calibration. When merging HER2 regions we checked that they belonged to the same level-1 HER to ensure that they share similar environmental characteristics at the large scale. In the end, a partition of France into 75 entities (HER2 or pool of HER2) was considered for this study (median area: 4990 km²; Fig. 1).

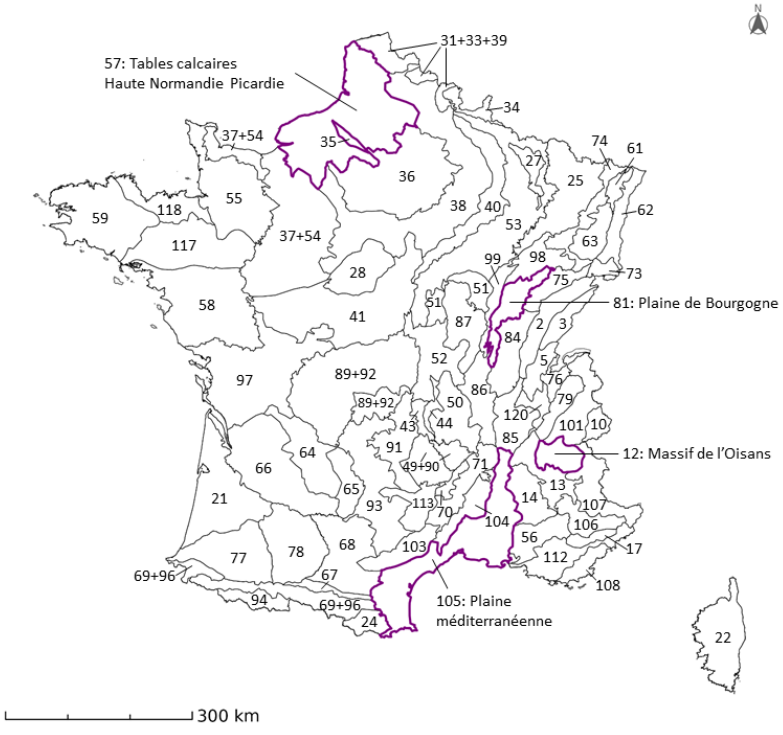

Figure 1: Delineation of level 2 Hydro-Ecoregions (HER2) across France. The four HER2 that are used for illustration in this study are highlighted in purple.

2.3 Modelling future discharge over France: the Explore2 project

Changes in the *PFI* over the 21st century are based on the large set of hydrological projections produced by the Explore2 project (Sauquet et al., in prep). The daily discharge projections were obtained at about 4000 simulation points distributed along the French river network, with a constraint on the minimum drainage area imposed by the spatial resolution of climate projections (64 km²) and another constraint of an even coverage across France. Most Explore2 simulation points were selected since data collected at these locations contribute to actual environmental monitoring or water management issues.

Explore2 is a multi-model simulation experiment, involving nine different hydrological models (HM), but some of them are restricted to regional applications. On average, each simulation point has discharge projections simulated by four HM (Interquartile Q1 and Q3 (IQ): 3-5). Finally, with the objective of predicting flow intermittence at the national scale, we select the five models with the largest simulation domain: CTRIP (Decharme et al., 2019), GRSD (De Lavenne et al., 2016), J2000

https://doi.org/10.5194/egusphere-2024-2737
Preprint. Discussion started: 19 September 2024

(Morel et al., 2023), ORCHIDEE (Huang et al., 2024), and SMASH (Jay-Allemand et al., 2020). The Explore2 project considers only natural flows, although some of the HMs involved in the project have the capability of including human-induced influences. The hydrological model evaluation was performed using an extended dataset of near-pristine catchments (Strohmenger et al., 2023). This observation-based simulation for each HM was carried out for the period 1976-2022 using the French near-surface SAFRAN meteorological reanalysis (Vidal et al. 2010) as input. In addition, these HM included in Explore2 have been evaluated on the common period of availability 1976-2019 (Sauquet et al., in prep). After validation, the HM are forced by an ensemble dataset from 17 pairs of Global and Regional Climate Models (GCM-RCM) corrected by the statistical adjustment method ADAMONT (Verfaillie et al., 2018) for both historical (1976-2004) and future climate scenarios RCP 2.6, 4.5 and 8.5 (2005-2100; Appendix Sect. A). In the end, the bias-corrected climate projections were used as inputs for the hydrological models: 10 GCM-RCM projections (resp. 9 and 17) are used for the RCP2.6 scenario (resp. RCP4.5 and RCP8.5). The baseline period H0 is set to 1976-2005 and used thereafter for analysing changes in IRES behaviour. Overall, the hydrological projections used thereafter to predict *PFI* result from combinations RCP-GCM-RCM-HM.

3 Modelling framework

3.1 Linking intermittence to stream discharge at the HER2 scale

The empirical method suggested by Beaufort et al. (2018; Eq. (4)) is applied here to estimate the Probability of Flow Intermittence (*PFI*) at the scale of HER2 regions. Under current climate conditions, $PFI_h(j)$ values are given by the percentage of ONDE sites with "dry conditions" for each HER2 (h) and each campaign date (j) (Fig. 2). This percentage of dry ONDE sites is considered as representative of the regional *PFI*. Subsequently, a logistic regression model is calibrated for each HER2 in order to estimate *PFI* values for day j (Eq. (1)).

$$PFI_h(j) = \frac{e^{\beta_{0\cdot HER2_h}+\beta_{1\cdot HER2_h}\times F_{Q\cdot HER2_h}(j)}}{1+e^{\beta_{0\cdot HER2_h}+\beta_{1\cdot HER2_h}\times F_{Q\cdot HER2_h}(j)}}, \quad (1)$$

where $\beta_{0\cdot HER2_h}$ and $\beta_{1\cdot HER2_h}$ are respectively the logistic regression intercept and slope coefficient associated with the predictor $F_{Q\cdot HER2_h}$.

The model uses the mean non-exceedance frequencies of discharge $F_{Q\cdot HER2_h}(j)$ as explanatory variable (Eq. (2)). $F_{Q.HER2h}$ is regarded as a proxy for characterising current wet versus dry hydrological conditions at the regional scale. More specifically, for each specific date (j) corresponding to an ONDE field campaign and each HER2 (h), the daily empirical non-exceedance frequencies of discharge are spatially averaged over all available n streams whose drainage areas intersect the HER2 of interest (weighted by their drainage area) and temporally averaged over the period $[j-6; j]$. This seven-day window allows the integration of non-simultaneous response times caused by propagation times in the underground and the river networks (the choice for a seven-day window is the result of an optimisation process, see Appendix Sect. B).

$$F_{Q\cdot HER2_h}(j) = \frac{1}{7\times n}\sum_{k=j-6}^{j}\sum_{s=1}^{n} F_Q(k,s) \quad (2)$$

https://doi.org/10.5194/egusphere-2024-2737
Preprint. Discussion started: 19 September 2024

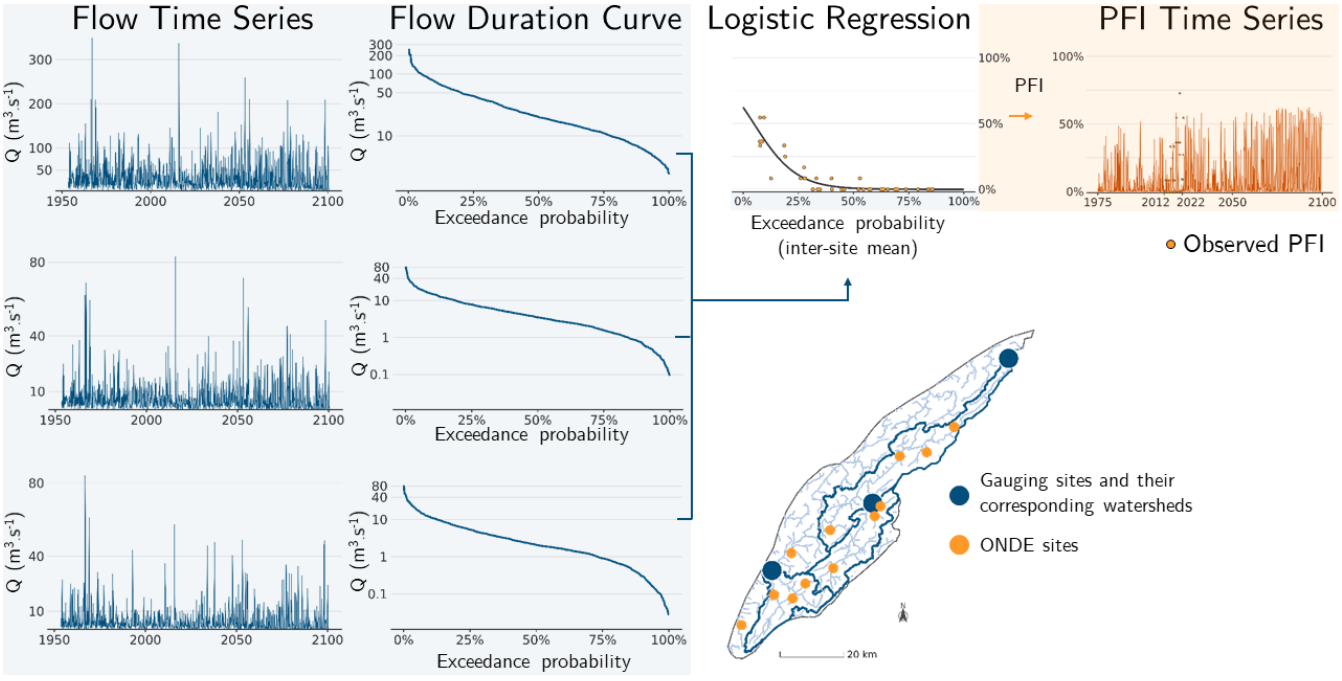

Figure 2: Schematic view of the approach adapted to derive the regional Probability of Flow Intermittence (*PFI*) from ONDE sites and gauging stations within a given HER2

3.2 Calibrating the PFI logistic regression models using observed daily discharge data

The daily discharge data used in the calculation of $F_{Q.HER2h}$ were compiled using gauging station records from the French reference hydrologic network HydroPortail (Leleu et al., 2014) (www.hydro.eaufrance.fr). The set of gauging stations were selected on the basis of three different criteria:

- Daily discharge data must be available during the ONDE field campaigns, i.e., within the $[j-10;j+10]$ interval centred on 25th of each month from May to September, for the years 2012 to 2022.
- The human disturbance to flow must be minimal at the gauging stations.
- All selected gauging stations must have a drainage area of less than 2000 km². Large gauged basins with a high Strahler order have been discarded since they are unlikely to behave in the same way as headwater streams.

This selection process results in a final dataset including 1008 stations (Fig. 3). The flow duration curve of each gauging station is computed using its entire available discharge time series.

3.3 Assessing the performance of PFI logistic regression models under current climate

Logistic regression models are preliminarily fitted between 2012 and 2022 using observed discharge data. Several cross-validation schemes are then considered to test the robustness of these models. A leave-one-year-out cross-validation is first carried out by excluding one year at a time from the training dataset, learning from the data of the remaining years and then

https://doi.org/10.5194/egusphere-2024-2737
Preprint. Discussion started: 19 September 2024

making estimations for the excluded year. The robustness under different climate conditions is also assessed through differential split-sample test (DSST; Dakhlaoui et al., 2017), which is a k-fold cross-validations performed on three distinct groups of hydrological years categorized as dry, intermediate, or wet (Appendix Sect. C). The years are discriminated selected according to the aridity index (Barrow, 1992), which is one on the main drivers of flow intermittence at the global scale (Sauquet et al., 2021).

The model performance is assessed using several skill scores: the bias (to detect underestimation or overestimation), the mean absolute error (MAE, to quantify the magnitude of prediction errors), and the root-mean-square error (RMSE, which provides a quadratic estimation that assigns relatively higher weight to large errors). Additionally, the Nash-Sutcliffe model efficiency coefficient (NSE) is computed to compare the variance of the estimation error to the variance of the observed time series (Nash and Sutcliffe, 1970). The Kling-Gupta Efficiency (KGE) complements the NSE metric as KGE is the Euclidean distance between observed and estimated *PFI*, computed using the coordinates of bias, standard deviation, and correlation (Gupta et al., 2009). The Leave One Year Out analysis results are obtained by averaging the validation metrics computed for each year.

3.4 Simulating PFI in a changing climate

The modelling framework suggested by (Beaufort et al., 2018; Sauquet et al., 2021) was applied to the 75 HER2s under regional climate projections to assess the potential impact of climate change on flow intermittence dynamics.

Discharge data derived from the Explore2 database are used as input for the logistic regression models introduced in Sect. 2.1.3. However, not all the stations in the HydroPortail database have been simulated by the HMs. To overcome this co-location problem, the choice was made to identify the simulation points closest to the 1008 gauging stations selected for the diagnosis in Section 2.1.4 (Fig. 3). The conditions of the application experiment are thus similar to the ones of the diagnostic experiment. A constraint was applied to ensure that no simulation point was assigned multiple times, unless there was no alternative point within a 50 km distance from the gauging station (Appendix Sect. D). This selection was made independently for each hydrological model. Only 483 points were assigned for the J2000 model because this model simulates streamflow only for the Loire and Rhône river basins.

https://doi.org/10.5194/egusphere-2024-2737
Preprint. Discussion started: 19 September 2024

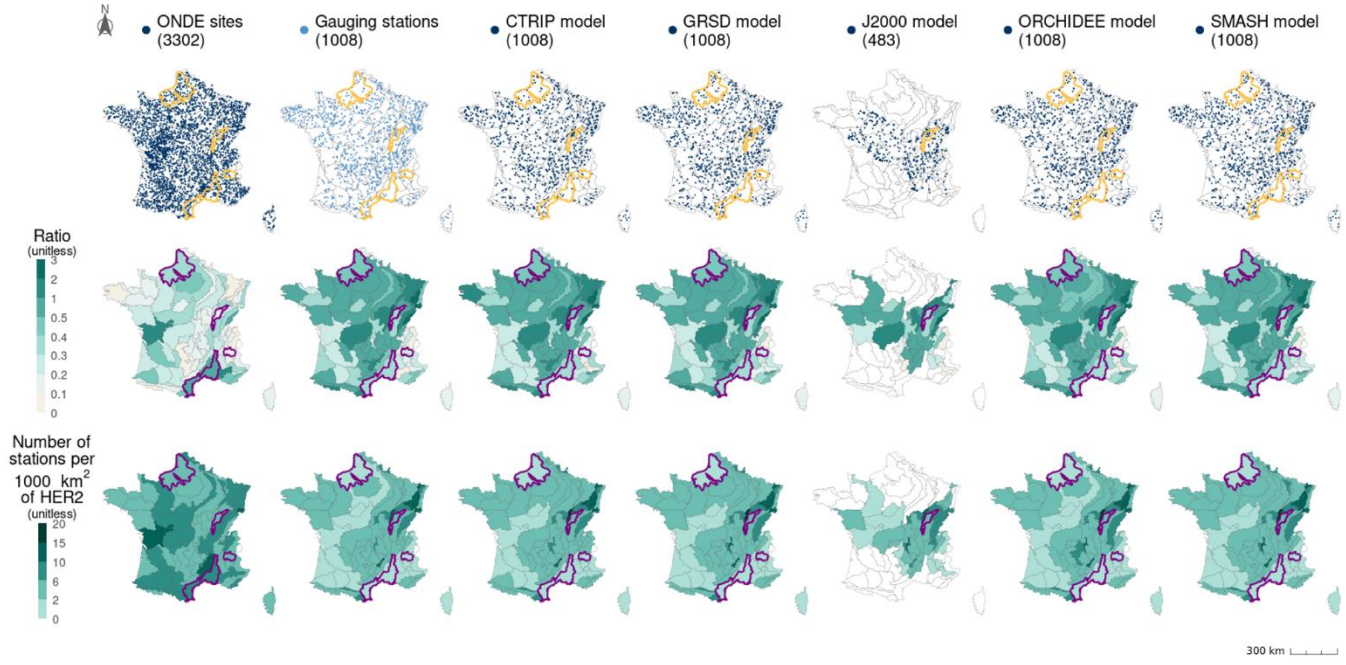

Figure 3: Location of the 3302 ONDE sites, the 1008 gauging stations selected from the HydroPortail database, and the Explore2 simulation points selected for each HM (line 1). Maps on the second and third line respectively show the ratio between the sum of the catchment areas defined by the gauging stations or the simulation points and the surface area of the HER2 they intersect (line 2), and the density of gauging stations or simulation points (line 3).

Applying empirical formulas (i.e., fitted using observed discharges) to simulated discharges may lead to poor estimates of *PFI* due to bias in the modelling chains. Thus, before being applied to future climate conditions, Eq. (1) needs to be recalibrated with past discharges simulated by each HM (here discharges simulated by the different HMs using SAFRAN reanalysis data available during the period 2012-2022 are used). In addition, to avoid problems of extrapolating exceedance frequency for values outside the range of flows simulated with SAFRAN, we decided to build a synthetic flow time series with a period length of 169 years, by combining available daily discharge data simulated with SAFRAN over the period 1976-2022 with projected discharge data over the period 1976-2100. This concatenation was made independently for each modelling chain RCP-GCM-RCM-HM at each simulation point. Finally, each synthetic discharge time series generated by a specific RCP-GCM-RCM-HM modelling chain results in a flow duration curve which is used thereafter to calibrate the logistic regression (Eq. (1)). The resulting logistic regressions are evaluated for each HM using the median of the bias, MAE, RMSE, NSE, and KGE skill scores over all RCP-GCM-RCM modelling chains.

3.5 Assessing changes in PFI and associated uncertainties

We compare *PFI* between a reference period H0 (1976-2005), and medium-term (H1, 2041-2070) as well as long-term (H2, 2070-2099) horizons. Results are presented at the HER2 scale across France and illustrated in more details for four contrasted HER2s: “Haute Normandie Picardie” (HER2-57, North, oceanic temperate climate), “Plaine de Bourgogne” (HER2-81,

https://doi.org/10.5194/egusphere-2024-2737
Preprint. Discussion started: 19 September 2024

Northeast, continental temperate climate), "Massif de l'Oisans" (HER2-12, Alps, mountainous climate), and "Plaine méditerranéenne" (HER2-105, Southeast, Mediterranean climate). In the rest of the article, "dry periods" of HER2s are defined as the period of the year when *PFI* is greater than 20%. For each HER2, the changes in intensity and seasonality of flow intermittence for H1 and H2 relative to H0, are characterized using the mean daily *PFI* between July and October ($mPFI_{7\text{-}10}$), and the median of the first and last days (respectively, *Tf* and *Tl*) of the year with *PFI* exceeding 20%.

The analysis of the uncertainty propagation in the modelling framework is examined using the QUALYPSO method, applied to the national average of $mPFI_{7\text{-}10}$ ($mPFI_{7\text{-}10}[France]$), weighted by HER2 areas and obtained under RCP 2.6, 4.5 and 8.5 climate change scenarios (Evin et al., 2019; Evin et al., 2021). The QUALYPSO method is used to characterise the changes in $mPFI_{7\text{-}10}[France]$ by estimating its ensemble mean over all the projections, as well as the total uncertainty associated with this set of projections, the contribution of the various sources of uncertainty (RCP, GCM, RCM, HM, residual and internal climate variability) to the total uncertainty and the main effect of each individual model and its contribution to the total uncertainty. The contribution of one specific model is estimated by the difference between the mean of all modelling chains considering the model at hand and the ensemble mean.

A multi-model index of agreement (*MIA*) is also computed on $mPFI_{7\text{-}10}$ time series to highlight convergence in changes over the projections (Tramblay and Somot, 2018):

$$MIA = \frac{1}{n}\sum_{k=1}^{n} i_k, \quad (3)$$

where n is the number of projections, $i_k = 1$ for a significant positive trend of the $mPFI_{7\text{-}10}$ according to the Mann-Kendall test (with $\alpha = 0.1$), $i_k = -1$ for a significant negative trend and $i_k = 0$ for no significant trend.

4 Results

4.1 Data pre-processing

The study involves 75 HER2s with a median surface area of 4990 km², of which more than 20% (17/75) have a surface area greater than 10000 km². The HER2s were the subject of ONDE field campaigns from May to September between 2012 and 2022, thus resulting in 4125 campaigns. A total of 78 campaigns are excluded from the analysis due to their failure to cover more than 75% of the monitoring stations within a given HER2. Thus, the data exclusion rate from the ONDE network is less than 2%, leaving 4047 field campaigns with usable data.

The 3302 ONDE sites are located in headwaters while gauging stations in France are monitoring medium size catchments (Van Meerveld et al., 2020). In addition, all Explore2 simulation sites have a drainage area larger than 64 km². Unsurprisingly, there is little overlap between the distribution of areas drained by ONDE sites (median: 24 km²; IQ: 12-50) and those drained

https://doi.org/10.5194/egusphere-2024-2737
Preprint. Discussion started: 19 September 2024

by the two sets of 1008 gauging stations (median: 173 km²; IQ: 85-396) and 1008 simulation points (median: 178 km²; IQ: 95-400) (Appendix Sect. E). ONDE sites, gauging stations and simulation points are located at similar elevations (overall median: 168 m; IQ: 75-308). The drainage areas of ONDE sites, gauging stations and simulation points represent respectively a median coverage of 21% (IQR: 15-35), 54% (IQR: 31-94) and 55% (IQR: 32-96) of the HER2 areas. This corresponds to a median number of 6.1 sites (IQR: 5-8), 3.6 stations (IQR: 1.9-5.7) and 3.7 simulation points (IQR: 2-6) per 1000 km² of HER2 (Fig. 3). These statistics highlight the question of representativeness of the ONDE sites despite the even coverage of the ONDE network.

4.2 Model performance

The logistic regressions calibrated using observed flows accurately predict PFI under current climate conditions (Fig. 4; Appendix Sect. G). The median performance across HER2s is, for example, 0.85 for KGE (IQ: 0.77-0.89) and 0.79 for NSE (IQ: 0.64-0.84) when the leave-one-year-out cross-validation is considered. The KGE skill score exceeds 80% in 50 out of 75 HER2 and the bias is very low. The best performances are observed in sedimentary plains and in Aquitaine while lower performances are obtained in mountainous areas such as the Alps, the Massif Central and the Pyrenees. The mean absolute error and RMSE show that the largest absolute deviations between observations and predictions occur in the southeastern part of France. This result is consistent with previous findings (e.g. Fig. 3 in Sauquet et al., 2021): (1) the performance of the logistic regressions is partly correlated with the level of intermittence, and (2) no-flow conditions which mainly occur in winter due to freezing in the Alps are not captured by the ONDE network. Observed values of $mPFI_{7\text{-}10}$ range between 3 and 37% (median: 14.3%) across France while values of $mPFI_{7\text{-}10}$ obtained with SAFRAN range between 2 and 37 % (median: 14.4%). The modelling approach is able to reproduce the spatial pattern of flow intermittence (Fig. 4), although the results obtained with the DSST show less satisfactory performance (Appendix Sect. G). The two skill scores KGE and NSE are sensitive to wet, intermediate and dry conditions while the other skill scores show no major change. The values of RMSE and MAE skill scores do not increase much when the calibration dataset is stratified based on climate conditions, which indicates that the proposed model is quite robust to climate fluctuations. The bias, however, indicates an underestimation of PFI in the southwest and in the north during dry years. This lower performance is partly due to a reduced number of years used for calibration purposes, and to the difficulty to extrapolate the logistic regression equations under unobserved climate conditions.

https://doi.org/10.5194/egusphere-2024-2737
Preprint. Discussion started: 19 September 2024

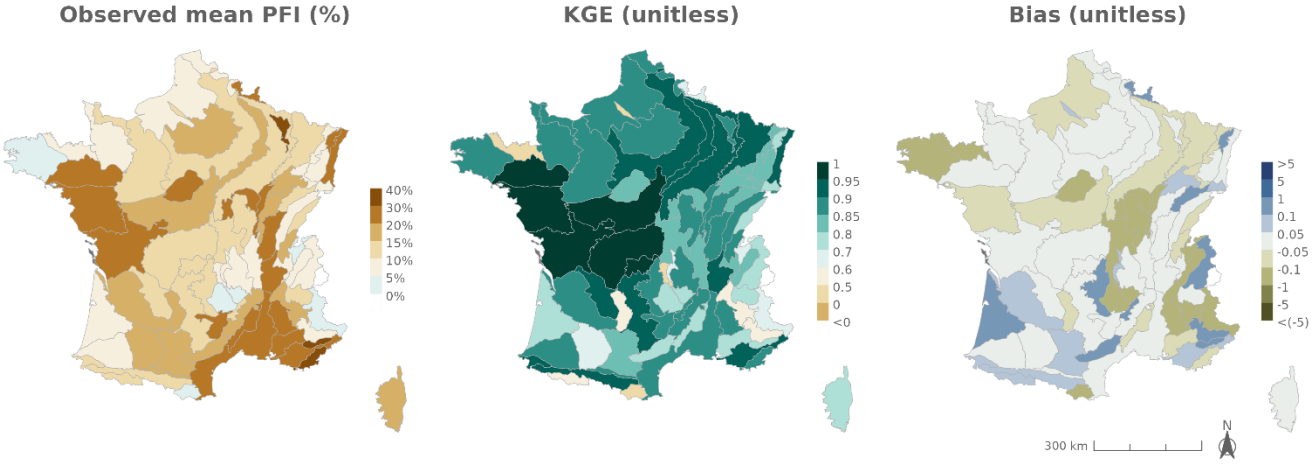

Figure 4: Leave-One-Year-Out cross-validation assessing the calibration of the logistic regressions using discharge measurements from gauging stations. From letf to right: observed mean PFI measured during the calibration period (2012-2022, left), Kling-Gupta Efficiency (KGE, center) and absolute bias of PFI predictions (right).

The logistic regressions fitted with discharge data simulated by HM also accurately reconstruct PFI from May to September. Compared to the results obtained with observed discharge data, the performance is slightly lower due to the inherent imperfections of the SAFRAN reanalysis compared to the observed climate (Fig. 5, 6; Table 1; Appendix Sect. H). The inter-HER2 and inter-projections median estimated $mPFI_{7\text{-}10}$ across France is 11.3-13.5% depending on HM, which is close to the 14.3% value (IQR: 8.4-20.3) derived from the ONDE network. The KGE is slightly lower but exceeds 80% in more than half of the HER2 using the CTRIP (38/75), SMASH (38/75), and GRSD (43/75) models. The inter-HER2 median of the NSE skill score (calculated for all RCP-GCM-RCM modelling chains and for each of these three HM) indicates that between 71% and 74% of the variance in $mPFI_{7\text{-}10}$ is explained by the logistic regressions. The other skill scores do not show a loss of performance (KGE between 0.80 and 0.81; MAE between 0.04 and 0.05, and RMSE between 0.06 and 0.07) when comparing the results of the Leave-One-Year-Out cross-validation obtained using observed and simulated discharge data. Lower performance is observed with the ORCHIDEE and J2000 models, as the KGE exceeds 80% in only 7/75 and 5/37 HER2, respectively. Their median KGE (0.60 and 0.69, respectively), NSE (0.49 and 0.62), MAE (0.06), and RMSE (0.08 and 0.09) are lower than the values obtained during calibration using observed flow data, indicating that these two hydrological models seem less sensitive.

Regardless of the HM of interest, the maps of skill scores show spatial patterns that are consistent with the results obtained with observed discharge data (Fig. 6; Appendix Sect. H). Both NSE and KGE remain high in the sedimentary plains and the southern part of the country, while they are less favorable in mountainous regions (Alps, Massif Central, and Pyrenees). An overestimation persists in the southwestern part of France, while underestimations of *PFI* values are found in the northwestern, northern, and southeastern parts of France, and are especially pronounced during dry years. The models also successfully

https://doi.org/10.5194/egusphere-2024-2737
Preprint. Discussion started: 19 September 2024

reproduce the inter-annual variability of *PFI*, particularly the alternation of dry (e.g., 2019) and wet (e.g., 2015) years (Fig. 5; Appendix Sect. G). Thus, the modelling chains demonstrate their ability to simulate *PFI* over the period 2012–2022 and are therefore deemed reliable to attempt projecting changes in flow intermittence under modified climate conditions. However, note that *PFI* values are slightly underestimated when the logistic regressions are calibrated on the driest years and applied than those used for calibration. This suggests that our future projections are likely to be biased in the same way, since the calibration is based on current conditions before applying the regression models to a potentially drier future climate.

.

HM	NSE (unitless)	KGE (unitless)	MAE (unitless)	RMSE (unitless)
Observed discharge data Leave One Year Out (2012-2022)	0.79 (IQ: 0.64-0.84)	0.85 (IQ: 0.77-0.89)	0.10 (IQ: 0.06-0.13)	0.07 (IQ: 0.05-0.09)
CTRIP	0.74 (IQ: 0.61-0.80)	0.80 (IQ: 0.69-0.85)	0.05 (IQ: 0.04-0.07)	0.07 (IQ: 0.05-0.10)
GRSD	0.74 (IQ: 0.64-0.80)	0.81 (IQ: 0.71-0.86)	0.04 (IQ: 0.03-0.06)	0.06 (IQ: 0.04-0.08)
J2000	0.62 (IQ: 0.52-0.71)	0.69 (IQ: 0.63-0.79)	0.06 (IQ: 0.04-0.09)	0.09 (IQ: 0.07-0.13)
ORCHIDEE	0.49 (IQ: 0.39-0.63)	0.60 (IQ: 0.50-0.72)	0.06 (IQ: 0.04-0.09)	0.08 (IQ: 0.06-0.11)
SMASH	0.71 (IQ: 0.65-0.80)	0.80 (IQ: 0.72-0.86)	0.04 (IQ: 0.03-0.06)	0.06 (IQ: 0.05-0.08)

Table 1: Evaluation of the logistic regressions calibrated using observed discharge data (results of the cross validation) and using flows simulated by the CTRIP, GRSD, ORCHIDEE and SMASH hydrological models. Statistics of the skill scores are summarized by medians and interquartile ranges (IQ, into brackets) across all HER2s.

https://doi.org/10.5194/egusphere-2024-2737
Preprint. Discussion started: 19 September 2024

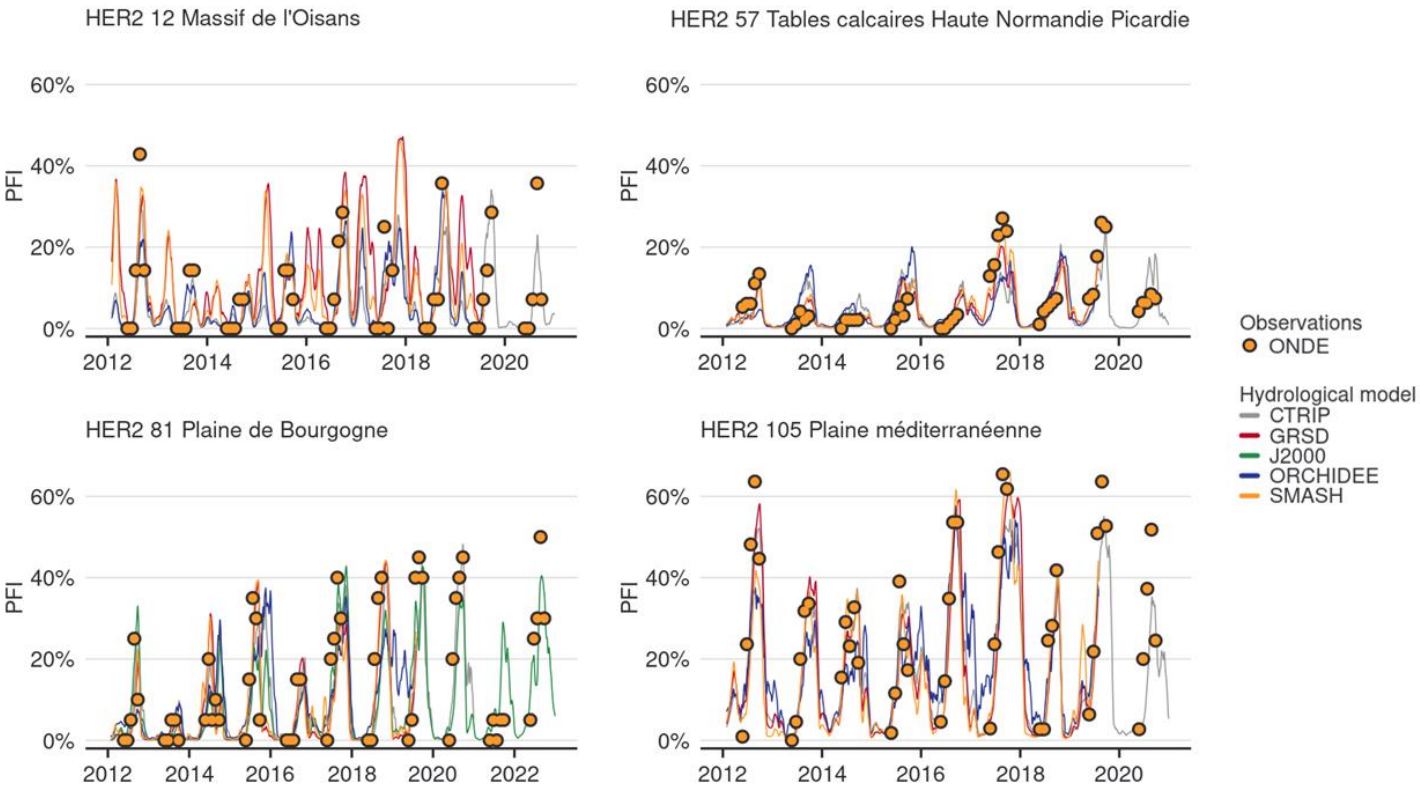

Figure 5: Time series of *PFI* for the four HER2s selected for illustrative purposes. Dots and lines are observed *PFI* derived from the ONDE network and estimated *PFI* computed by the logistic regressions using simulated discharge by HMs, respectively.

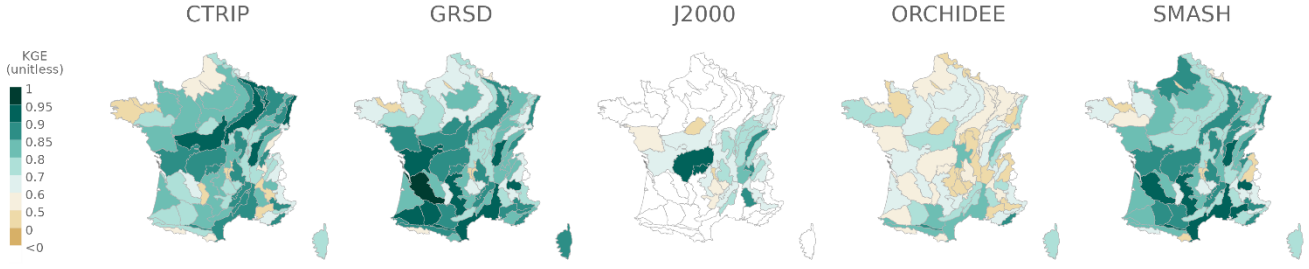

Figure 6: Kling-Gupta Efficiency (KGE) assessing the calibration of logistic regression using discharge simulated by HM with SAFRAN-based simulations available during the 2012-2022 period

4.3 Flow intermittence projections

The logistic regressions fitted for each HER2 are applied to derive the *PFI* values from the historical (1976-2004) and future (2005-2100) discharges simulated by the HMs forced by RCP-GCM-RCM climate projections over the period 1976-2100.

https://doi.org/10.5194/egusphere-2024-2737
Preprint. Discussion started: 19 September 2024

Figure 7 shows the evolution of $mPFI_{7\text{-}10}$ and of the start date *(Tf)* and end date *(Tl)* of the dry period for H1 and H2 compared to H0. The results are illustrated in Fig. 7 with the median projection given by the GRSD model (see Appendix Sect. H for other models) under RCP2.6, RCP4.5, and RCP8.5 climate scenarios. Table 2 details the same results for the four HER2 under RCP8.5.

Overall, the average *PFI* shows an increase, indicating a gradual intensification of dry periods over the 21st century under the RCP 4.5 and RCP 8.5 scenarios. The inter-HER2 and inter-projections median of $mPFI_{7\text{-}10}$ calculated at the national scale ($mPFI_{7\text{-}10}[France]$) for the baseline period H0 ranges from 10 to 12% depending on the HM. However, the median projection of $mPFI_{7\text{-}10}$ during H0 is higher than 20% in 12 to 20 of the 75 HER2s (depending on the HM), althought it does not exceed 42% in any HER2. In contrast, under RCP 8.5, $mPFI_{7\text{-}10}[France]$ could reach values between 13 and 21% in the mid-term of the century H1 and between 16 and 29% by the end of the century H2. By this time, six HER2s could have inter-projections median of $mPFI_{7\text{-}10}$ exceeding 50% according to at least two HM: four in the south-east of France; one in the southwest; and one in the northwest of France. Under RCP 4.5, changes are more moderate by the end of the century H2, with $mPFI_{7\text{-}10}[France]$ ranging between 14 and 20%. The spatial pattern of the changes is not uniform but looks similar between RCP 8.5 and RCP4.5. A strengthening divide between the south-west and the north-east of the country is projected. Regions already prone to intermittence are expected to experience an increase in this phenomenon under both emission scenarios. The ratio of the ensemble median of $mPFI_{7\text{-}10}$ at the end of the century compared to the baseline period evolves around 1.4 for RCP 4.5 and 1.9 for RCP 8.5. Mountainous regions see the intensity of summer dry periods increase but remain relatively spared.

Shifts of the start and the end of the dry period are partly correlated with changes in $mPFI_{7\text{-}10}$ (Fig. 7). It appears that climate change results in both earlier and later dry periods in a fairly symmetrical manner: dry periods are advanced and extended, but with different sensitivities structured along a north-south gradient. Under RCP 8.5 climate conditions, the dry periods are projected to get (on median) longer in southern France at the end of the century. According to at least two HM, the highest shifts of *Tf* or *Tl* could exceed 5 weeks in several mountainous HER2 (four HER2 in the Alps, three in the Pyrenees, two in the Jura). In contrast in the northern part of France, the dry periods could be advanced and extended by only one or two weeks, as observed in HER2-81 “Plaine de Bourgogne” (Table 2). HER2 28 could be one of the most affected in the north due to its impermeable clay-sandy formations, which differs from the neighbouring sedimentary formations. One can note a change in seasonality for the HER2-12 “Massif de l’Oisans” located in the Alps (Fig. 8, example with the GRSD hydrological model). No-flow events were concentrated in winter (retention of water in the snow cover) during the historical period. Under climate change, temperature will be higher leading to less snowfall and more runoff in the river network during winter. The river flow regime will be more sensitive to losses by evapotranspiration and finally no-flow conditions will likely occur in summer by the end of the 21st century.

https://doi.org/10.5194/egusphere-2024-2737
Preprint. Discussion started: 19 September 2024

HER2	Period	$mPFI_{7\text{-}10}$ (%)			*Tf* (date)			*Tl* (date)		
		Min	Median	Max	Min	Median	Max	Min	Median	Max
Haute Normandie Picardie (57)	H0	8	13	15	30/07	22/08	05/10	22/09	30/10	04/12
	H1	7	14	23	15/07	24/08	11/10	11/10	10/11	16/12
	H2	5	16	34	04/06	21/08	23/11	16/10	12/11	23/12
Plaine de Bourgogne (81)	H0	12	19	22	10/07	31/07	18/08	18/09	27/10	16/12
	H1	11	23	34	09/07	02/08	01/09	02/10	04/11	29/12
	H2	10	27	47	21/06	22/07	03/09	04/10	08/11	31/12
Massif de l'Oisans (12)	H0	6	11	17	26/07	23/08	06/10	18/09	19/11	17/03
	H1	11	21	38	27/06	01/08	01/09	23/09	30/10	03/12
	H2	12	29	52	29/05	12/07	21/08	28/09	02/11	15/12
Plaine méditerranéenne (105)	H0	14	25	29	22/06	17/07	16/08	22/09	23/10	17/12
	H1	9	31	46	29/05	11/07	28/08	25/09	01/11	25/12
	H2	9	41	57	02/04	16/06	30/08	02/10	13/11	01/01

Table 2: Statistics of flow intermittence characteristics for the four illustrative HER2s under RCP 8.5. The minimum (min), median and maximum (max) are the ensemble minimum, median and maximum across all the projections and hydrological models.

https://doi.org/10.5194/egusphere-2024-2737
Preprint. Discussion started: 19 September 2024

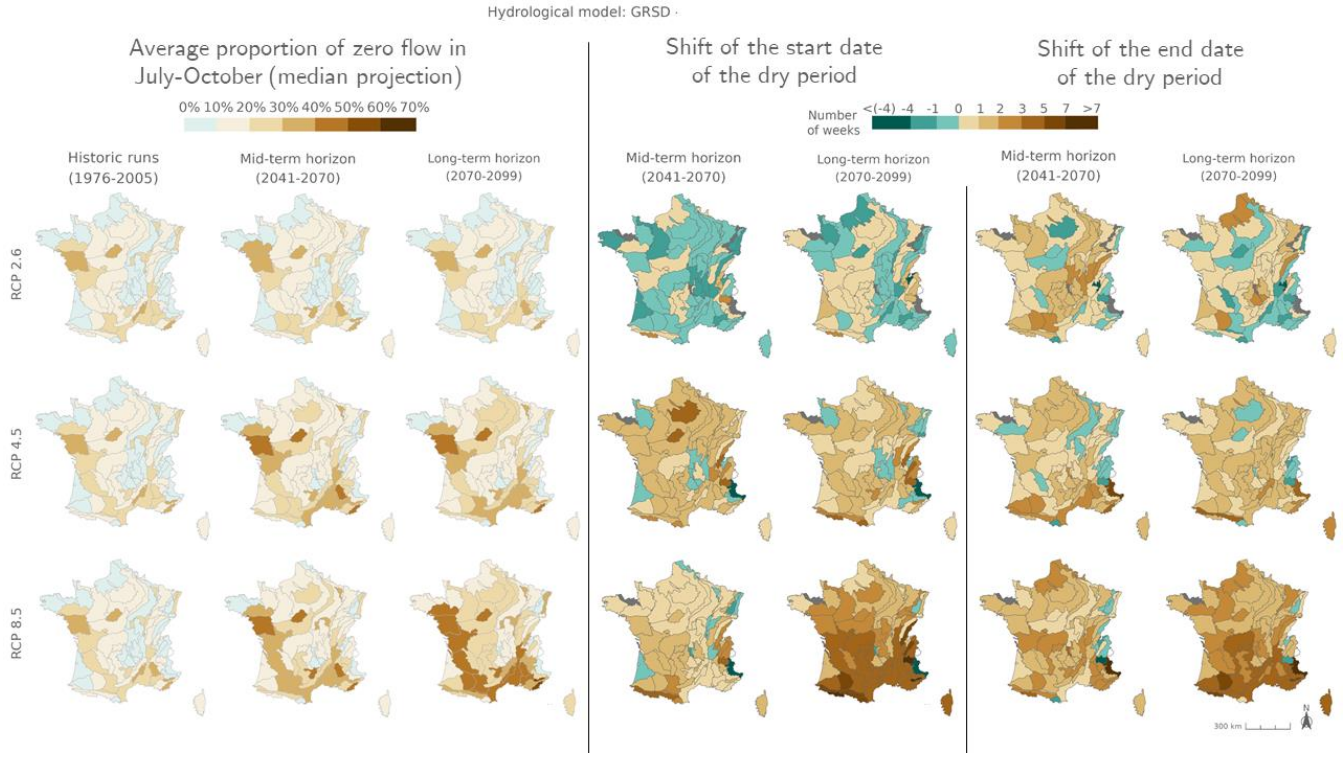

Figure 7: Ensemble median of changes in *mPFI*$_{7\text{-}10}$ (columns 1 to 3), and ensemble median shift of the start date *Tf* (columns 4 and 5) and the end date *Tl* (columns 6 and 7) of the dry period over the two periods H1 and H2 under the three RCPs for the GRSD hydrological model, relative to the baseline period H0. The shift, expressed in week, takes a positive value when the duration of the dry period increases. Grey HER2s had no period with a *PFI* >20% during the reference period. The same results are available for the other HM in Appendix Sect. H.

https://doi.org/10.5194/egusphere-2024-2737
Preprint. Discussion started: 19 September 2024

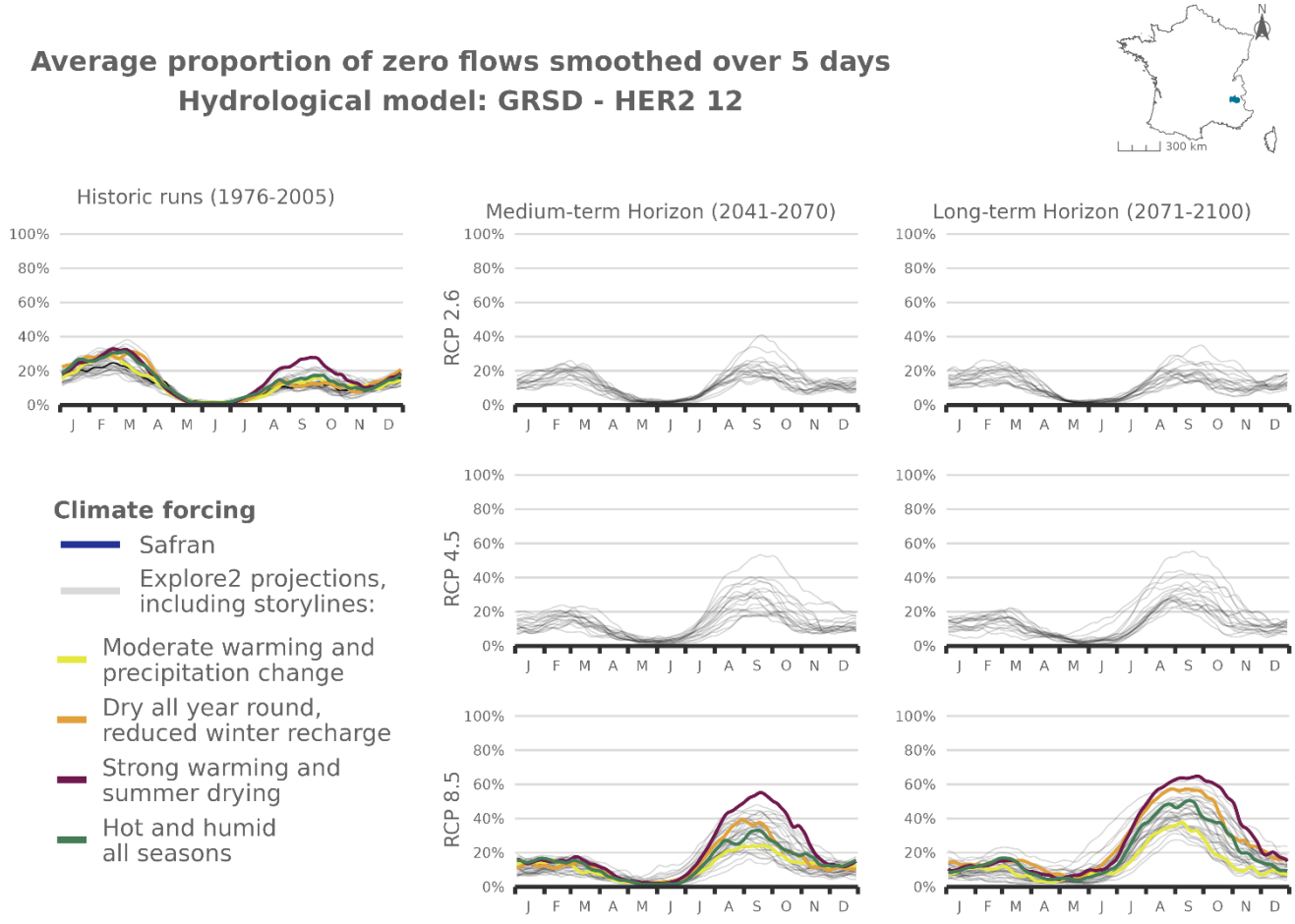

Figure 8: Seasonal pattern of *PFI* for the periods H0, H1 and H2 under RCP 2.6, 4.5 and 8.5 scenarios for GRSD hydrological models in the Alps (HER2 12). The storylines highlighted in this figure are introduced in Appendix Sect. H. The same results are available for HER2s 57, 81 and 105, and for the other HM in Appendix Sect. H.

4.4 Uncertainty analysis

Figure 9 illustrates the results of the uncertainty analysis, showing the variability of $mPFI_{7\text{-}10}[France]$ throughout the 21st century. These results confirm that dry conditions may occur more frequently in a changing climate, with 22% projected increase in $mPFI_{7\text{-}10}[France]$ by the end of the century. The total variability of $mPFI_{7\text{-}10}[France]$ over all projections results from the accumulation of uncertainties related to RCP scenarios, GCMs and RCMs, residual variability, and internal variability. The confidence interval, and therefore the extent of change, increases over the course of the 21st century due to the divergent results of the modelling chain. This finding is consistent with studies using a similar methodology to assess the uncertainty of panels of flow projections (Evin et al., 2019; Aitken et al., 2023).

https://doi.org/10.5194/egusphere-2024-2737
Preprint. Discussion started: 19 September 2024

The contribution of each component to the total uncertainty varies over time. The fraction of total variance due to residual variability is small and remains stable over time. The main part of the variability in climate change responses is thus explained by RCP, GCM, RCM and HM. In addition, the contribution of the internal variability is highly predominant and represents more than 75% of the total uncertainty until the mid-century. This contribution then decreases with time as the total uncertainty increases. It becomes less than 50% of the total uncertainty by the end of the century but remains the greatest contributor to the total uncertainty over the whole simulation period.

Regarding the spatial distribution of the different contributions to the total uncertainty, it appears that climate data are predominant in the uncertainty, and that they are distributed in a spatially heterogeneous manner over France. The uncertainty related to the RCP scenarios increases over time and becomes predominant in the south, surpassing uncertainties related to other steps of the modelling chain (GCM, RCM, and HM). In the mountainous regions, differences between results obtained with RCP4.5 and RCP8.5 are clearer by the end of the century, leading to a contribution of RCP to the total uncertainty reaching 20% at the end of the century. In northern France, the contribution of RCP to the uncertainty is lower compared to HM, GCM, or RCM contributions. Uncertainty related to hydrological models is also spatially structured, with greater uncertainty in the northwestern part of France.

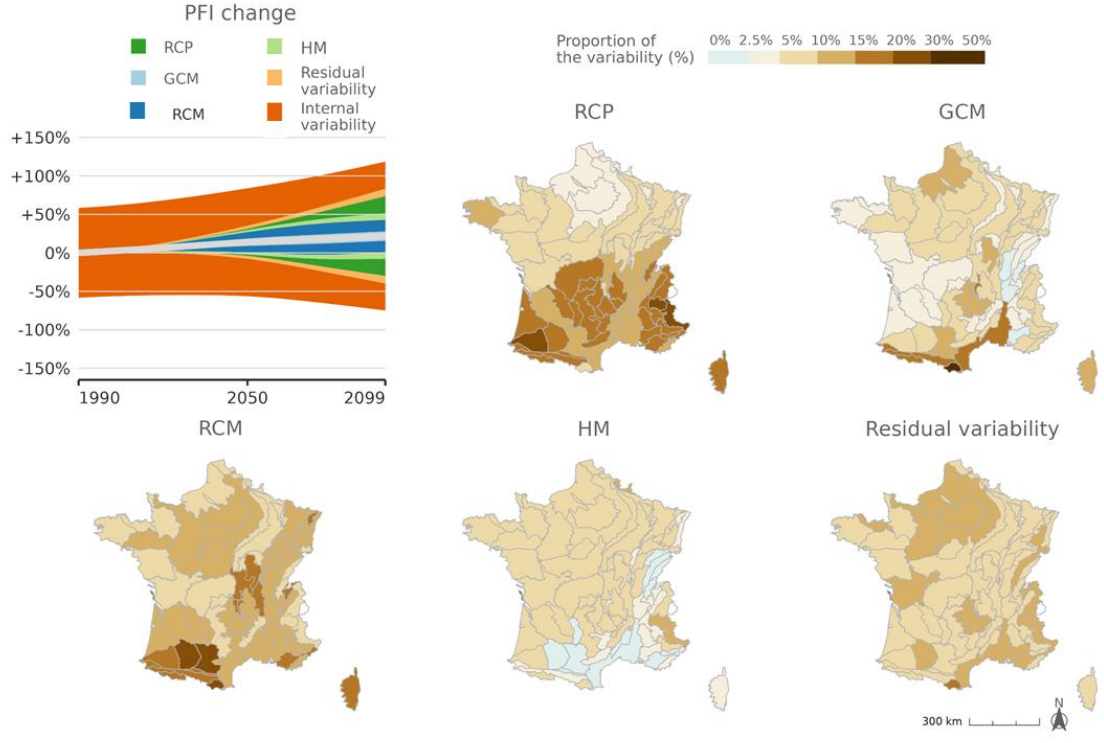

Figure 9: Decomposition of the effects contributing to the variance of projections for relative changes (unitless) of *mPFI$_{7\text{-}10}$[France]*. The grey line and the coloured areas show the climate change response and the contribution of time for each step of the modelling chain to the 90% confidence interval, respectively. For each model uncertainty and internal variability component, the vertical extent of the corresponding area is proportional to the fraction of total uncertainty explained by the component.

https://doi.org/10.5194/egusphere-2024-2737
Preprint. Discussion started: 19 September 2024

4.5 Agreement between changes

Despite uncertainties about the intensity of change, *PFI* projections still show a good degree of convergence in the direction of change when considering all climate projections driving each hydrological model individually, as well as in the overall convergence of *PFI* projections (Fig. 10). *MIA* values are first calculated independently for each MH, before all projections are combined for multi-model assessment.

Figure 10 highlights spatial contrasts of the *MIA* multi-model approach: unsurprisingly, the projections of $mPFI_{7\text{-}10}$ are more uncertain in the northern part of France. The climate change signal on the proportion of dry periods is not homogeneous across France, with significant uncertainties remaining for the northern part.

The agreement of projections is high for the GRSD and SMASH models across France (*MIA* values close to +100% under RCP8.5 in Fig. 10 and +80% under RCP4.5, see Appendix Sect. I). In contrast, CTRIP, J2000, and ORCHIDEE suggest contrasted regional impacts of climate change on PFI under RCP4.5, with a reduction of the $mPFI_{7\text{-}10}$ in the northern part of France, indicating a differentiated sensitivity of hydrological models to climate changes. This trend is also observed for ORCHIDEE under RCP8.5, while the other models agree on an increasing drying.

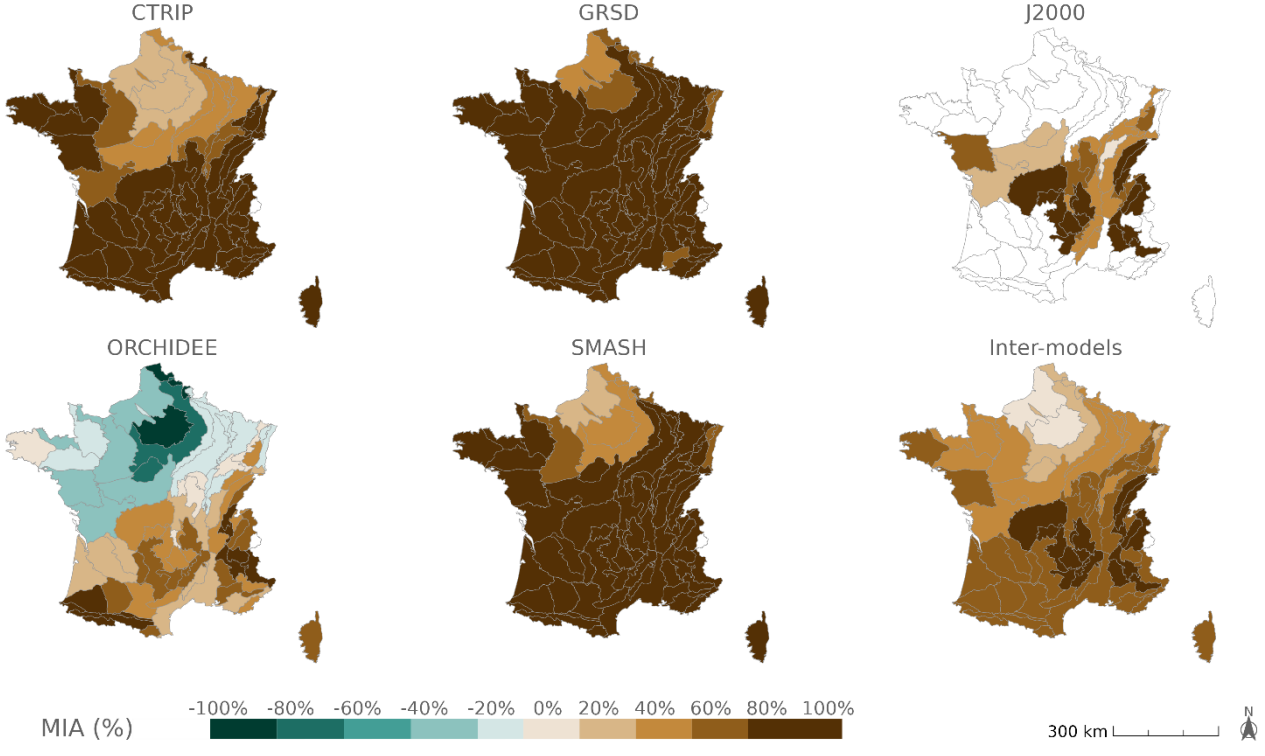

Figure 10: Agreement between projections of $mPFI_{7\text{-}10}$ for each hydrological model and inter-model agreement on the change signal of $mPFI_{7\text{-}10}$ under the RCP 8.5 scenario.

https://doi.org/10.5194/egusphere-2024-2737
Preprint. Discussion started: 19 September 2024

5 Discussion

5.1 Modelling framework and assumptions

This study presents projections of the *PFI* in headwater streams by HER2 in France over the 21st century. It extends the previous analysis of Sauquet et al. (2021) on the 2012-2018 period by exploiting an extensive national dataset of stream intermittence observations collected on low-order streams (3302 observation sites), which are the most affected by shifts from perennial to intermittent flows (Reynolds et al., 2015; Dhungel et al., 2016). For the first time, we project the future evolution of the *PFI* using discharge data obtained from 5 hydrological models with conceptual (GRSD, SMASH), surface (CTRIP, ORCHIDEE), or process-oriented distributed (J2000) structures, under a multitude of possible climate scenarios informed by 17 pairs of CMIP5 GCM-RCM models.

The results of this study should be interpreted within the context of its underlying assumptions. Firstly, the study focuses on unregulated streams to characterize the "natural" hydrology (i.e., without considering water abstraction by anthropogenic activities or the impact of hydraulic engineering structures). This assumption was made in the Explore2 project, which provides the input streamflow simulations. Nevertheless, global water model simulations including direct human impacts by Döll and Zhang (2010) concluded that ecologically relevant flow characteristics will be more altered by climate change than by withdrawals and dams. However, we believe that quantitatively estimating the extent to which flow intermittence is due to direct anthropogenic stressors is important for improving our projections of flow intermittence as well as for decision-making in view to regulate and prevent water stress situations for populations.

Secondly, groundwater levels are not incorporated into the model, although they could potentially enhance the accuracy of the projections. Projections of groundwater levels have been produced by the Explore2 project but only for a limited area of France.

Thirdly, with only five annual discrete observations of streamflow intermittence over eleven years for the calibration of the logistic regression models, our ability to capture the full range of extremes and variability in these regression models remains imperfect. Yet, visual monitoring remains the most common technique for observing non-perennial streams. An alternative approach would be to consider citizen science to augment our database, although concerns about data reliability persist, in particular because past studies have shown participant agreement rates ranging from 46% to 70% (Scheller et al., 2024). Data scarcity necessitated conducting this analysis at the HER2 scale, which nonetheless represents a significant improvement of the spatial resolution by increasing the number of modelling subdomains from 22 to 75 compared to previous studies (Sauquet et al., 2021). In future work, a downscaling process could enhance the usability of PFI projections for local stakeholders in water management.

Fourthly, while projections of no-flow events often exhibit significant uncertainties when derived directly from discharge simulated by HMs (Evin et al., 2019; Aitken et al., 2023), this study illustrates how categorical and discrete (in space and time) field observations can be combined with conventional stream gauge data, to enhance the understanding of headwater stream

https://doi.org/10.5194/egusphere-2024-2737
Preprint. Discussion started: 19 September 2024

drying dynamics. In this way, despite the divergences between projections induced by climate data, the agreement within this multi-model approach is relatively strong, indicating a consensus toward increasing *PFI* throughout the 21st century.

5.2 A consistent signal across projections

This study confirms that logistic regressions properly capture the relationships between flows in large watersheds and the *PFI* of headwater streams. These regressions are calibrated and validated using discharge measurements from gauging stations, and subsequently using discharge simulated from SAFRAN climate data. Following this second calibration, projections based on regressions consistently indicate an increase in average *PFI* and a shift in the start and end dates of dry periods under RCP 4.5 and RCP 8.5 climate projections, suggesting a progressive intensification and extension of dry periods over the 21st century. These results are consistent with previous studies indicating a transition of many streams from perennial to intermittent regimes (Jaeger et al., 2014; Reynolds et al., 2015; Dhungel et al., 2016; Schneider et al., 2013). Rising temperatures attributed to climate change lead to an increased evapotranspiration and aridity, consequently resulting in an increase in dry streams (Tramblay et al., 2020; Zipper et al., 2021). In regions already affected by intermittence, an increase in the intensity and duration of drying periods is likely, a phenomenon also anticipated in other areas around the world (Jaeger et al., 2014; Dai et al., 2011). Increasing intermittence and decreasing flow rates are observed in catchment-scale studies: the fraction of time with zero discharge increases from 0.05% to 4.30% in a Swiss Alpine catchment between 2020–2040 and 2080–2100 (Halloran et al., 2023) while the no-flowing phase could extend by up to 12 days between 1980-2009 and 2030-2059 for a catchment in southern Italy (De Girolamo et al., 2022). This trend is also noticeable on a larger scale, as monitoring of gauging stations in five regions with Mediterranean climates around the world between 1980 and 2019 (Carlson et al., 2024) and over 452 rivers on the European continent between 1970 and 2010 (Tramblay et al., 2020) both show that approximately 30% of them have already experienced drier conditions due to climate change, with modified flow regimes or extended periods of drying.

5.3 Uncertainties in northern France

In the northern part of France, discrepancies between GCM-RCM-HM projections result in higher uncertainties in *PFI* projections and pronounced geographical contrasts on the multi-model-based *MIA* map (Fig. 10). These uncertainties primarily arise from uncertainties in future rainfall patterns in this region where the majority of Explore2 projections indicate an increase in winter rainfall and winter mean flows (for 8 out of 9 HMs) and a decrease in summer precipitation. The annual precipitation by the end of the century remains uncertain, due to the compensatory effect between increased winter recharge and an increased evapotranspiration. As a result, some hydrological models predict a shortening of the dry period for certain northern HER2 regions, including under RCP 8.5. Similar uncertainties are observed along the east coast of the USA, where precipitation changes could turn intermittent streams into perennial ones (Dhungel et al., 2016) while alternative climate change scenarios projected that by the 2040s, approximately half of the streams in Washington state would shift from snow-fed to rain-fed, resulting in reduced annual discharge (Reidy Liermann et al., 2012).

https://doi.org/10.5194/egusphere-2024-2737
Preprint. Discussion started: 19 September 2024

5.4 Transformation of the snowmelt regime in the Alps

The mountain ranges could be moderately affected by the increased probability of dry conditions, consistent with our previous modelling efforts (Sauquet et al., 2021), but our projections anticipate two specific phenomena in these regions. First, the Pyrenees are more affected than the other mountain ranges, with significant changes impacting the massif and the dependent basins in southwestern France. Additionally, Alpine HER2s will probably undergo hydrological regime changes. Higher winter temperatures will lead to reduced snowfall and snow-related intermittence. This snowpack reduction will also reduce groundwater recharge by spring melt. In addition, since soils tend to retain less water in summer due to more intense and brief rainstorms (Rutkowska et al., 2023), an increased summer intermittence is expected despite increasing summer precipitations. Using 16 hydrographic variables describing the magnitude, frequency, timing, duration, and rate of change of the flow regime at 59 primarily selected sites with a Strahler order of 5, Dhungel et al. (2016) also observed the reduction in the snowmelt regime at 2 Rocky Mountain sites under climate change. Halloran et al. (2023) also conclude that groundwater will play an increasingly important role in ensuring flow in alpine streams and that the shift from perennial to intermittent could occur for alpine streams over the course of the current century.

Furthermore, the reduction of the snowmelt regime in the Alps indicate that we can still make projections consistent with the literature beyond the calibration period (May to September). More generally, the hypothesis of temporal transferability of the models is a strong assumption in data exploitation, as it assumes that climate models, statistical adjustment methods and hydrological models can simulate the behaviour of the systems they represent in a future hydro-climatic context that is very different from the one in which they were developed (Evin et al., 2024). In this context, it is important to recall the risk that the projections may be underestimated, as demonstrated by the validation of logistic regressions calibrated on wetter years compared to dry years.

6 Conclusion

In conclusion, HMs often show weaknesses in characterizing low flows and their responses to climate change. This study and other work in progress (e.g. Döll et al., 2024) show that the simulation of intermittent rivers on a national or global scale is a complex subject with real scope for progress. Leveraging monthly monitoring of headwaters over ten summers, we calibrated logistic regressions to transform hydrological projections of large watersheds into regional proportions of flow intermittence for the 21st century. Under both RCP 4.5 and 8.5 scenarios, robust signals indicate an intensification of dry events, marked by increased *PFI* and longer dry periods throughout the year. These changes are projected to be more pronounced in southern France, with greater uncertainty in the northern half of the country. Mountain areas could remain relatively spared from summer dry periods but shifts in hydrological regimes are anticipated. By the end of the century under RCP8.5, dry stream phenomena along the Atlantic coast could surpass those currently observed in the Mediterranean region by the usual monitoring campaigns. The evolution of droughts and reduced water availability suggested by these results could lead to significant ecological impacts, including alterations in the structure and function of freshwater ecosystems (such as changes in microbial

https://doi.org/10.5194/egusphere-2024-2737
Preprint. Discussion started: 19 September 2024

activity and habitat loss), shifts in soil chemistry, increased carbon and solute fluxes, and sediment mobilization (Geris et al., 2015).

Appendix A: Explore2 modelling

Global Climate Model	Regional Climate Model	Histo-rical	RCP 2.6	RCP 4.5	RCP 8.5
CNRM-CERFACS-CNRM-CM5	CNRM-ALADIN6	×	×	×	×
CNRM-CERFACS-CNRM-CM5	KNMI-RACMO22E	×	×	×	×
CNRM-CERFACS-CNRM-CM5	MOHC-HadREM3-GA7-05	×	-	-	×
ICHEC-EC-EARTH	KNMI-RACMO22E	×	×	×	×
ICHEC-EC-EARTH	SMHI-RCA4	×	×	×	×
ICHEC-EC-EARTH	MOHC-HadREM3-GA7-05	×	×	-	×
MOHC-HadGEM2-ES	CNRM-ALADIN63	×	-	-	×
MOHC-HadGEM2-ES	CLMcom-CCLM4-8-17	×	-	×	×
MOHC-HadGEM2-ES	ICTP-RegCM4-6	×	×	-	×
MOHC-HadGEM2-ES	MOHC-HadREM3-GA7-05	×	×	-	×
IPSL-IPSL-CM5A-MR	DMI-HIRHAM5	×	-	-	×
IPSL-IPSL-CM5A-MR	SMHI-RCA4	×	-	×	×
IPSL-IPSL-CM5A-MR	IPSL-WRF381P	×	-	×	×
MPI-M-MPI-ESM-LR	CLMcom-CCLM4-8-17	×	×	×	×
MPI-M-MPI-ESM-LR	ICTP-RegCM4-6	×	×	-	×
MPI-M-MPI-ESM-LR	MPI-CSC-REMO2009	×	×	×	×
NCC-NorESM1-M	DMI-HIRHAM5	×	-	×	×
NCC-NorESM1-M	GERICS-REMO2015	×	×	×	×
NCC-NorESM1-M	IPSL-WRF381P	×	-	-	×

Table A1: Global and Regional Climate Models combinations driving the Explore2 Hydrological Models selected for PFI simulation in the 21st century

https://doi.org/10.5194/egusphere-2024-2737
Preprint. Discussion started: 19 September 2024

Appendix B: Sensitivity analysis of the duration of flow measurement interval used as input for the logistic regression to calculate the PFI

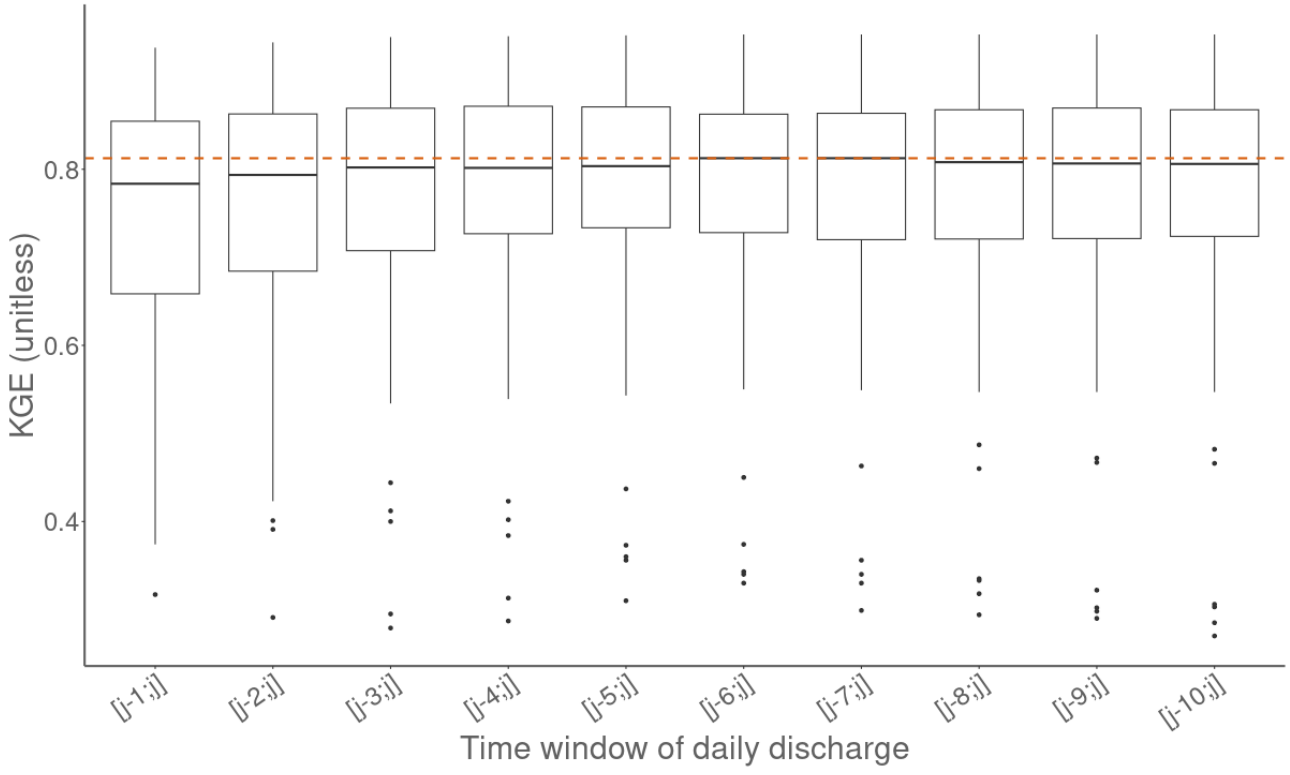

Figure B1: Kling-Gupta Efficiency (KGE) computed on results obtained by Leave One Year Out validations, testing the sensitivity to the time window of daily discharge used for calibrating the logistic regressions. Boxes represent the quartiles Q1 and Q3, the whiskers extend up to 1.5 times the IQR above Q3 and below Q1 and points located beyond the whiskers are displayed individually. The dashed line represents the median KGE of the [j-6;j] window

A sensitivity analysis was performed to fix the time window of daily discharge that optimizes the calibration of logistic regressions presented in Sect. 3.1. The calibration and validation were performed using the Leave One Year Out method, detailed in Sect. 3.3. The model performance was assessed using the Kling-Gupta Efficiency (KGE) (Gupta et al., 2009). The KGE values for the different HER2 are summarized using boxplots for each tested window size. The [j-6;j] window was selected because it corresponds to the highest median KGE score, the narrowest interquartile range, and the highest minimum KGE.

https://doi.org/10.5194/egusphere-2024-2737
Preprint. Discussion started: 19 September 2024

Appendix C: Separation of dataset based on dry, intermediate and wet years

The data from ONDE sites used for validation were collected between May and September over 11 years from 2012 to 2022. The robustness of the model was assessed through a validation process involving three sets of dry, intermediate, and wet years. For each test, model calibration was performed using the years excluded from the validation set.

The hydrological years are distributed into three equal groups of hydrological years (dry years, intermediate years and wet years) according to the annual aridity index, calculated at the national scale. The aridity index AI was given by the ratio between the total annual precipitation and potential evapotranspiration from August 1 of the previous year to July 31 of the current year (Barrow, 1992; Figure A2.1). A set of dry years was formed using hydrological years where potential evapotranspiration exceeded annual precipitation (AI < 1 for 2017, 2019, and 2022). Two sets were then created: the four years with AI greater than 1.4 were classified as wet years (2012, 2015, 2020 and 2021), and the remaining four years with AI between 1.15 and 1.37 were classified as intermediate years (2013, 2014, 2016, 2018).

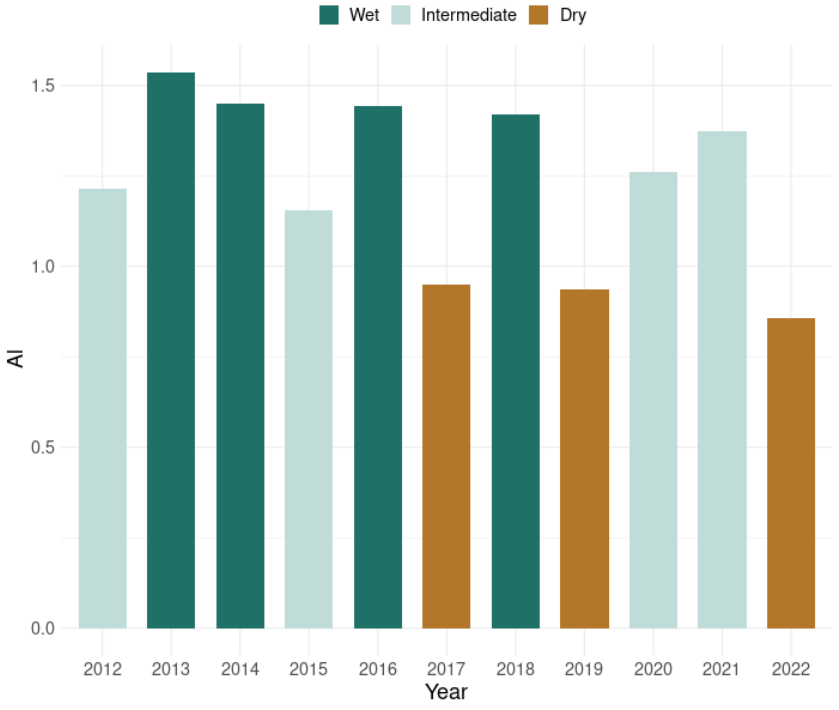

Figure C1: Aridity index for the hydrological years 2012 to 2022

https://doi.org/10.5194/egusphere-2024-2737
Preprint. Discussion started: 19 September 2024

Appendix D: Assignment of simulation points

After establishing the models' reliability through validation at secure monitoring stations, the next step involved extrapolation, which entailed linking these monitoring sites to the nearest simulation points in Explore 2 to project future hydrological scenarios while preserving the existing data structure. The proximity between the gauging station A and a simulation point in the Explore2 project is measured by the distance:

$$Dist(A,B) = \sqrt{\left(X(A) - X(B)\right)^2 + \left(Y(A) - Y(B)\right)^2 + (\alpha \times \Delta S_{rel})^2} \quad \text{(D1)}$$

Here, $(X(A), Y(A))$ and $(X(B), Y(B))$ are coordinates of A and B (in km), respectively, and $Surf(A)$and $Surf(B)$ are the drainage areas of A and B, respectively that are used to compute the relative difference between the drainage areas (absolute value).

$$\Delta S_{rel} = 2 \times \frac{|Surf(A) - Surf(B)|}{|Surf(A) + Surf(B)|} \quad \text{(D2)}$$

The coefficient α is used to balance the importance of geographical distance and the relative difference in surface and was set to 100.

https://doi.org/10.5194/egusphere-2024-2737
Preprint. Discussion started: 19 September 2024

Appendix E: Metadata

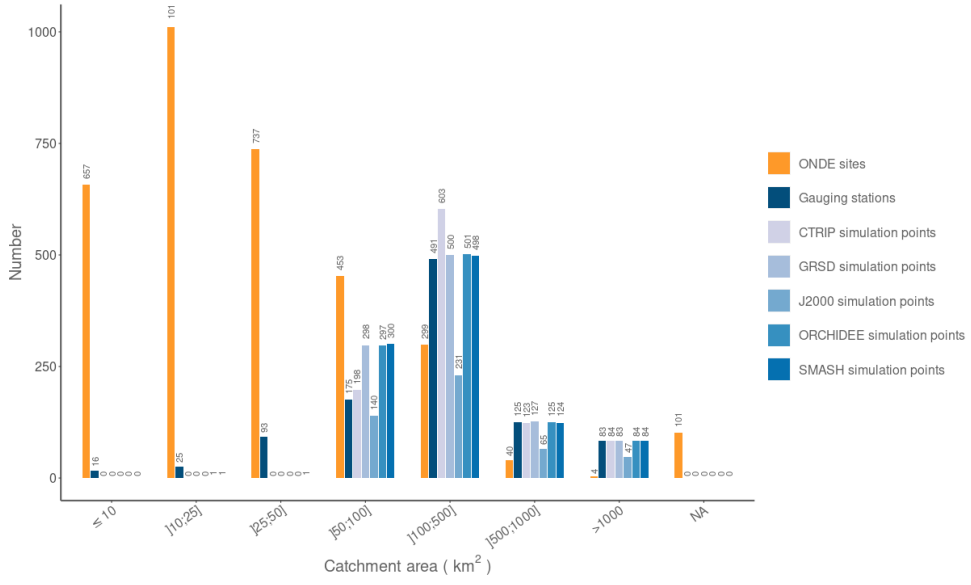

Figure E1: Frequency distribution of the number of ONDE sites, the 1008 gauging stations selected from the Hydroportail database, and the 1008 simulation points from Explore2 as a function of catchment area

NA: Missing values

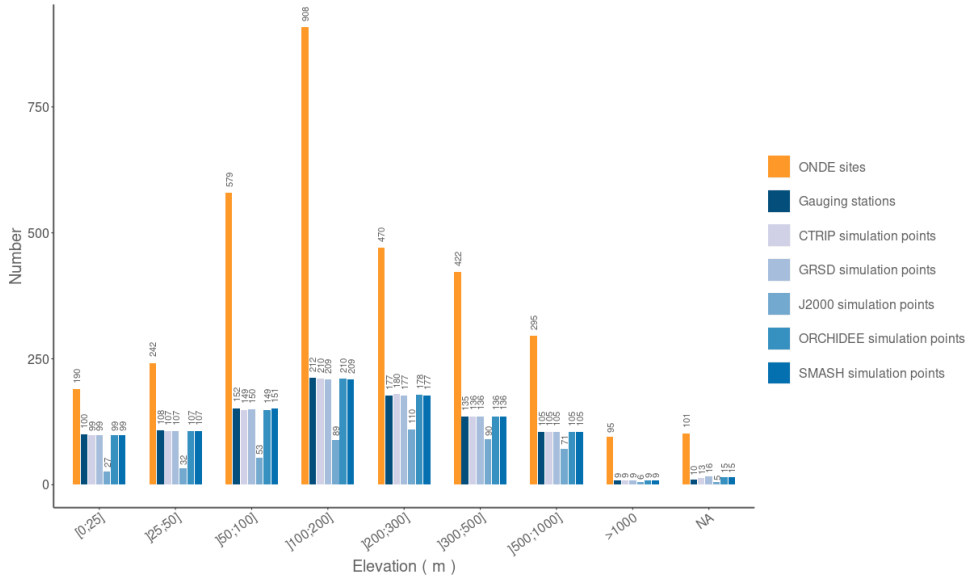

Figure E2: Frequency distribution of the number of ONDE sites, the 1008 gauging stations selected from the Hydroportail database, and the 1008 simulation points from Explore2 as a function of elevation

NA: Missing value

https://doi.org/10.5194/egusphere-2024-2737
Preprint. Discussion started: 19 September 2024

Appendix F: Model performance using observed discharge data from gauging stations as predictors

Over the observation period (2012-2022), logistic regression models estimate the PFI values at HER2 scale (Figure 4). The median observed PFI across all HER2 and all campaigns is 14.3% (IQR: 8.4-20.3) while the logistic regression models yield a median value of 14.4% (IQR: 8.5-20.4). With results of the leave-one-year-out cross-validation, the models explain 73% of the PFI variability according to the NSE (IQ: 64-84%) (Table 1; Figure F2), the KGE exceeds 80% in 50 out of 75 HER2 (Figure F2) and the bias is very low.

The models are also able to describe the inter-annual variability with the alternation of dry and wet years (Figure F1). The median KGE and NSE scores remain above 0.71 during k-fold validations considering dry, intermediate, and wet years for calibration. RMSE and MAE values do not increase much when the calibration dataset is stratified based on climate conditions, which indicates that the proposed model is quite robust to climate variations under current conditions.

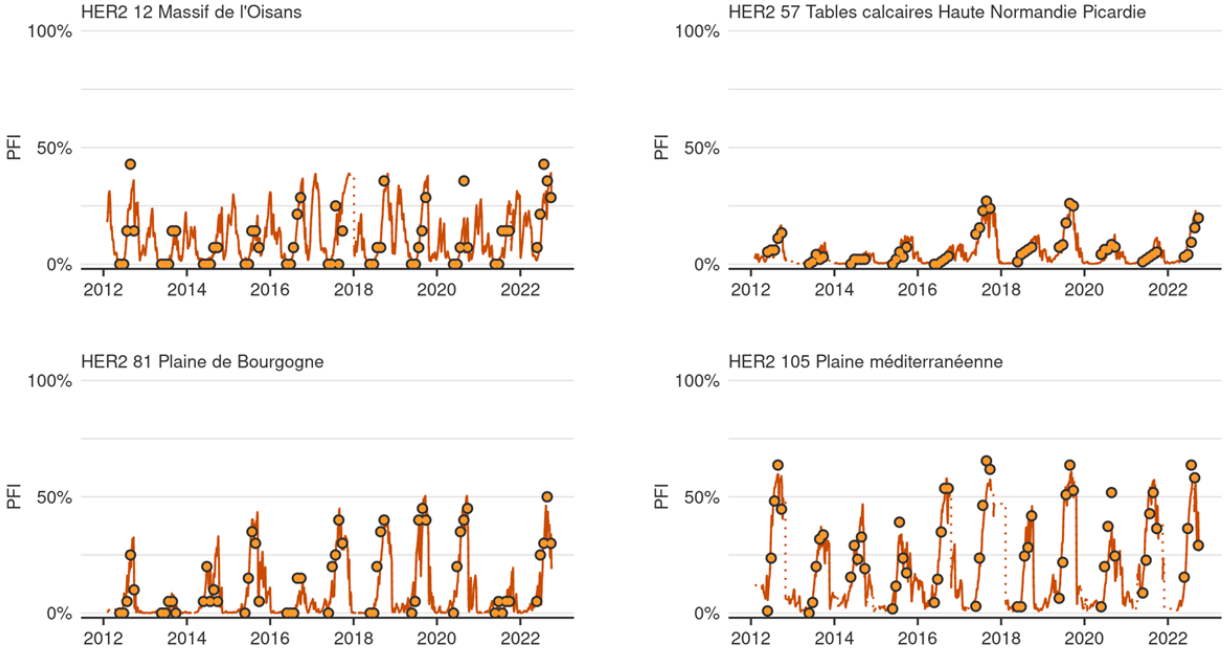

Figure F1: Time series of PFI in HER2 13, 57, 81 and 105. Points and lines respectively represent the PFI derived from the ONDE network and the PFI estimated by the logistic regression models using discharge data from gauging stations during the calibration period (2012-2022).

https://doi.org/10.5194/egusphere-2024-2737
Preprint. Discussion started: 19 September 2024

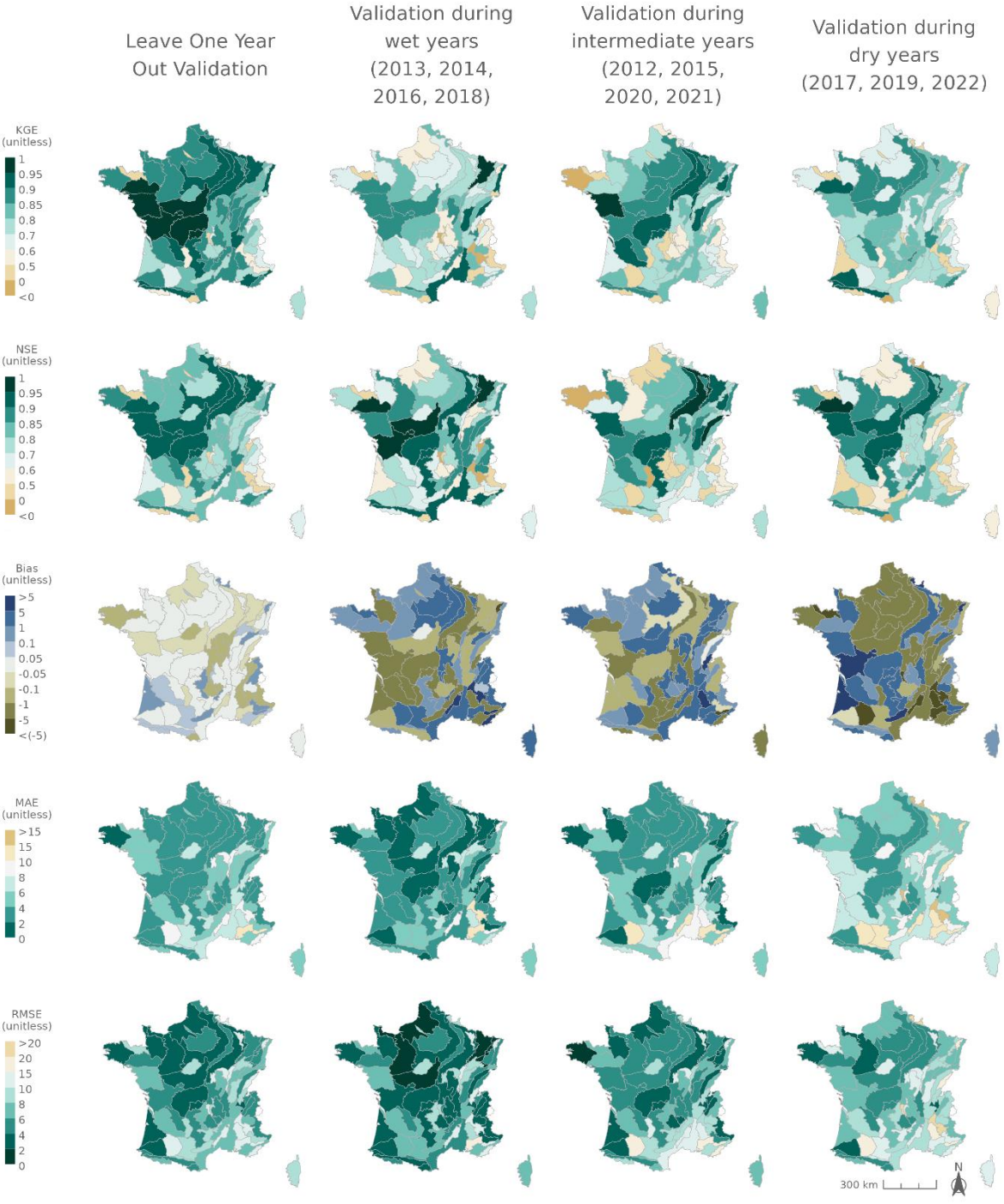

Figure F2: Kling-Gupta Efficiency (KGE, line 1), Nash–Sutcliffe model efficiency coefficient (NSE, line 2), Bias (line 3), Mean Absolute Error (MAE, line 4), Root-mean-square error (RMSE, line 5) over the calibration period (2012-2022)

https://doi.org/10.5194/egusphere-2024-2737
Preprint. Discussion started: 19 September 2024

Validation years	PFI observed on ONDE network (%)	Predicted PFI (%)	Nash Sutcliffe Efficiency (NSE, unitless)	Kling Gupta Efficiency (KGE, unitless)	Bias (unitless)	Mean Absolute Error (MAE, unitless)	Root Mean Square Error (RMSE, unitless)
Leave One Year Out (2012-2022)	14.3 IQ 8;20 min-max 3;37	14.4 IQ 9;20 min-max 2;37	0.79 IQ 0.6;0.8 min-max 0.2;0.9	0.85 IQ 0.8;0.9, min-max 0.3;1.0	-0.02 IQ -0.08;0.05 min-max -0.68;0.70	0.10 IQ 0.06;0.13 min-max 0.02;0.32	0.07 IQ 0.05;0.09 min-max 0.03;0.15
Wet years (2013, 2014, 2016, 2018)	8.3 IQ 5;15 min-max 1;29	8.7 IQ 5;13 min-max 0;35	0.76 IQ 0.6;0.9 min-max -1.7;1.0	0.71 IQ 0.6;0.8 min-max -4.0;1.0	0.17 IQ -1.23;1.25 min-max -7.09;7.32	0.05 IQ 0.03;0.09 min-max 0.01;0.23	0.05 IQ 0.03;0.08 min-max 0.02;0.15
Intermediate years (2012, 2015, 2020, 2021)	12.9 IQ 7;19 min-max 1;35	13.6 IQ 7;19 min-max 2;31	0.76 IQ 0.6;0.8 min-max -0.7;1.0	0.76 IQ 0.7;0.9 min-max -0.2;1.0	0.21 IQ -1.06;1.41 min-max -8.85;5.76	0.07 IQ 0.04;0.09 min-max 0;0.25	0.06 IQ 0.04;0.09 min-max 0;0.18
Dry years (2017, 2019, 2022)	21.5 IQ 14;30 min-max 2;51	21.4 IQ 14;32 min-max 4;49	0.7 IQ 0.5;0.8 min-max -0.1;1.0	0.75 IQ 0.6;0.8 min-max -0.6;0.9	-0.71 IQ -2.90;1.49 min-max -15.13;12.78	0.09 IQ 0.06;0.12 min-max 0.01;0.43	0.08 IQ 0.06;0.12 min-max 0.03;0.24

Table F1: Validation results of drying probability predictions at the HER2 scale using observed flows from the 1008 gauging stations from the HYDRO database. The results correspond to the inter-HER medians, quartiles, minimum and maximum values. The Leave One Year Out analysis results are obtained by averaging the validation metrics computed for each year.

Drying probability: Percentage of ONDE sites in a dry state computed for each HER2, averaged by month; FDC: Flow Duration Curve; IQ: Interquartile range; Min: minimum; Max: maximum

https://doi.org/10.5194/egusphere-2024-2737
Preprint. Discussion started: 19 September 2024

Appendix G: Model performance using discharge data simulated with SAFRAN

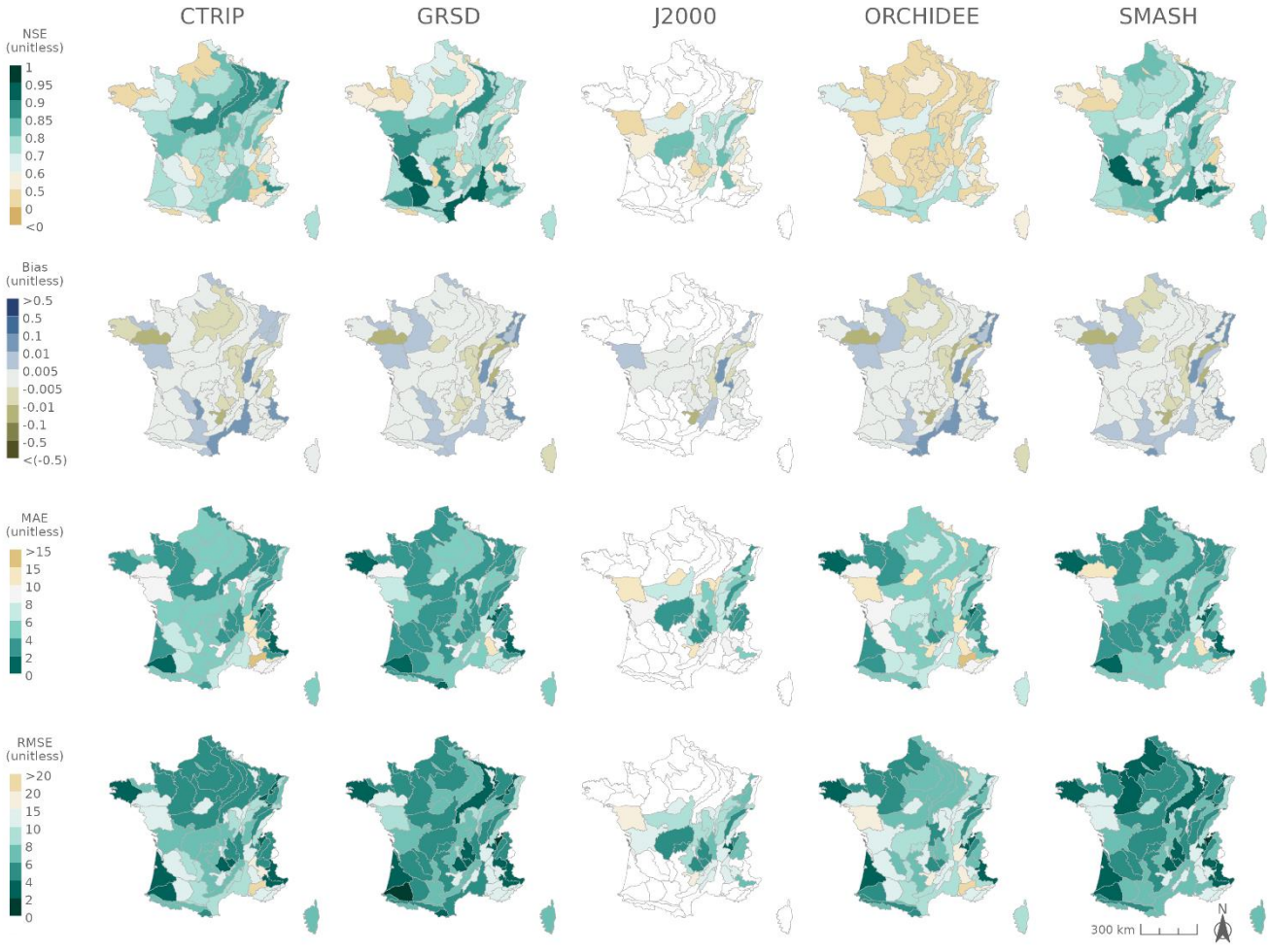

Figure G1: Nash–Sutcliffe model efficiency coefficient (NSE, line 1), bias (line 2), Mean Absolute Error (MAE, line 3), Root-mean-square error (RMSE, line 4) assessing the calibration of logistic regression using discharge data simulated with SAFRAN data available during the calibration period (2012-2022)

620

https://doi.org/10.5194/egusphere-2024-2737
Preprint. Discussion started: 19 September 2024

Appendix H: Application to 21st century PFI modelling

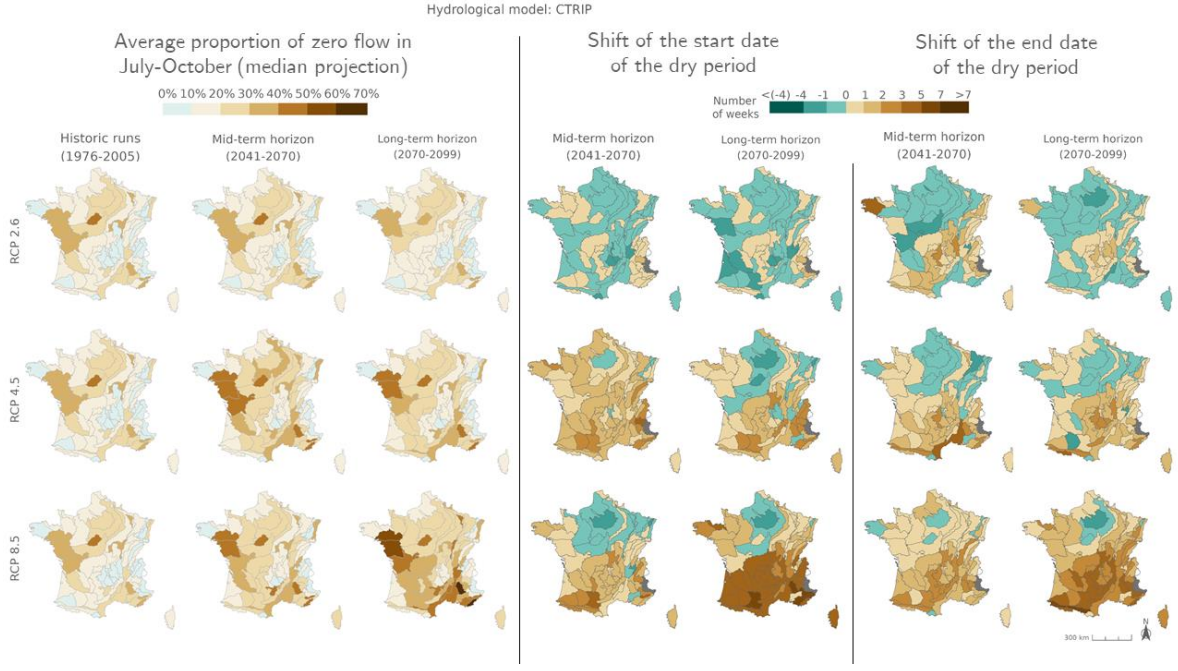

Figure H1: Ensemble median of changes in mPFI7-10 (columns 1 to 3), and ensemble median shift of the start date Ts (columns 4 and 5) and the end date Te (columns 6 and 7) of the dry period over the two periods H1 and H2 under the three RCPs for the CTRIP hydrological model, relative to the baseline period H0. The shift, expressed in week, takes one positive value when the duration of the dry period increases.

https://doi.org/10.5194/egusphere-2024-2737
Preprint. Discussion started: 19 September 2024

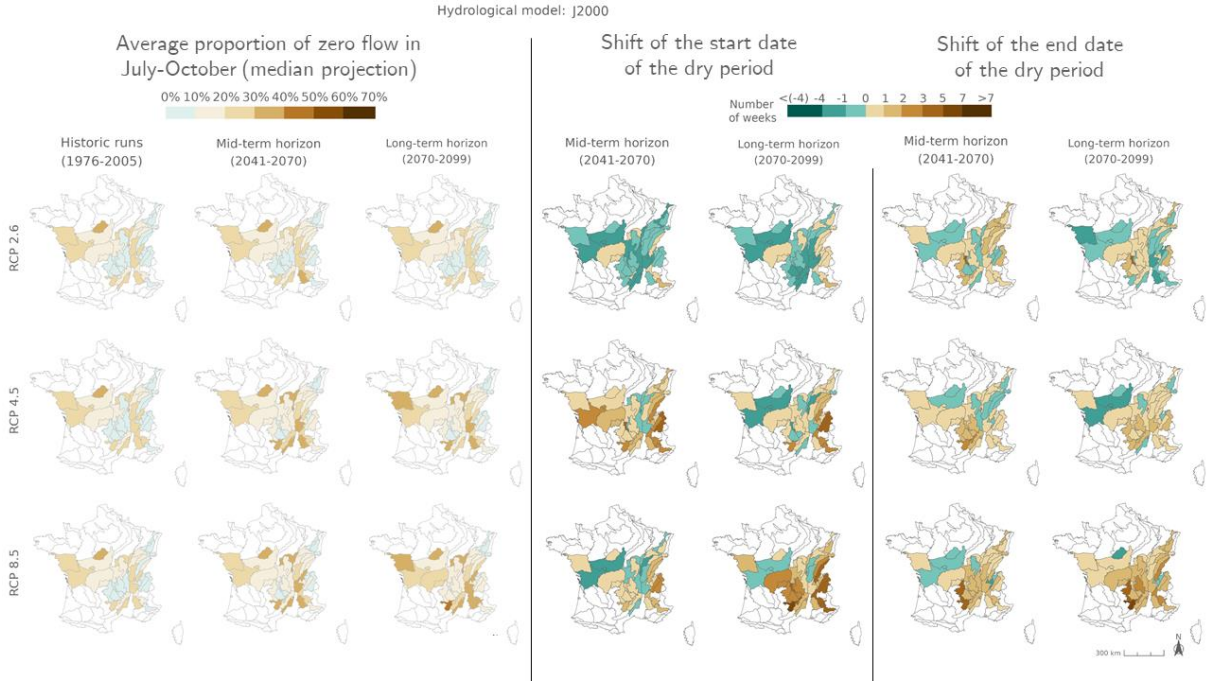

645

Figure H2: Ensemble median of changes in mPFI7-10 (columns 1 to 3), and ensemble median shift of the start date Ts (columns 4 and 5) and the end date Te (columns 6 and 7) of the dry period over the two periods H1 and H2 under the three RCPs for the J2000 hydrological model, relative to the baseline period H0. The shift, expressed in week, takes one positive value when the duration of the dry period increases.

650

655

660

https://doi.org/10.5194/egusphere-2024-2737
Preprint. Discussion started: 19 September 2024

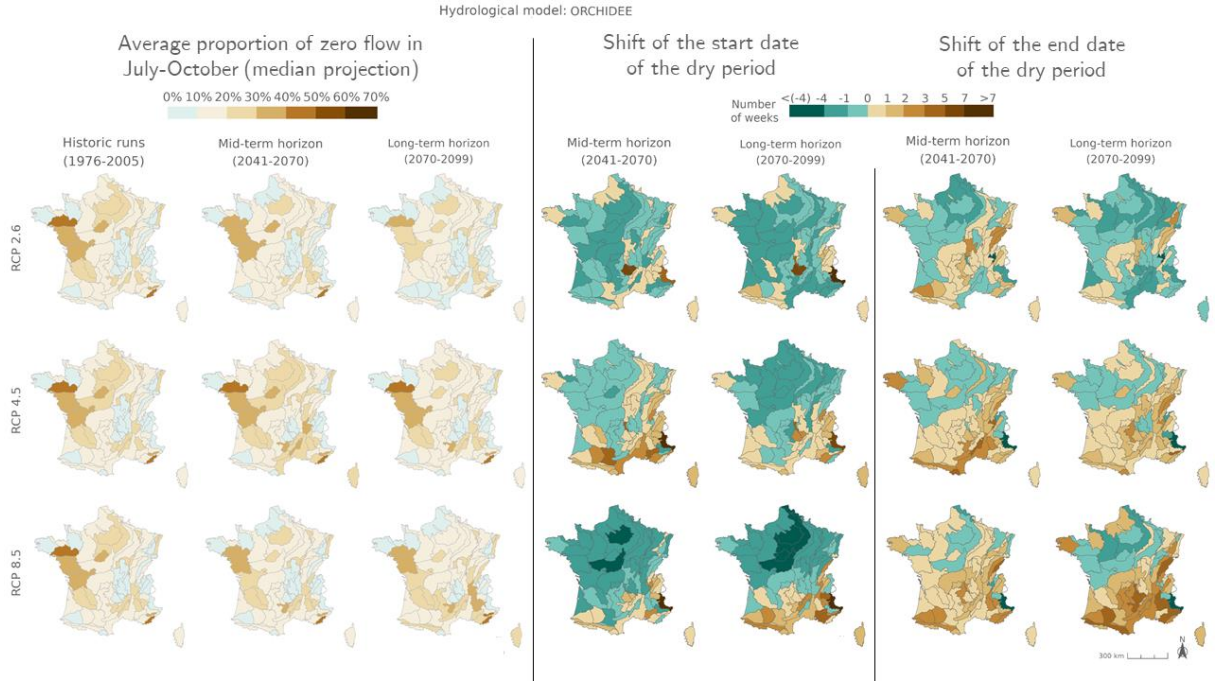

Figure H3: Ensemble median of changes in mPFI7-10 (columns 1 to 3), and ensemble median shift of the start date Ts (columns 4 and 5) and the end date Te (columns 6 and 7) of the dry period over the two periods H1 and H2 under the three RCPs for the ORCHIDEE hydrological model, relative to the baseline period H0. The shift, expressed in week, takes one positive value when the duration of the dry period increases.

https://doi.org/10.5194/egusphere-2024-2737
Preprint. Discussion started: 19 September 2024

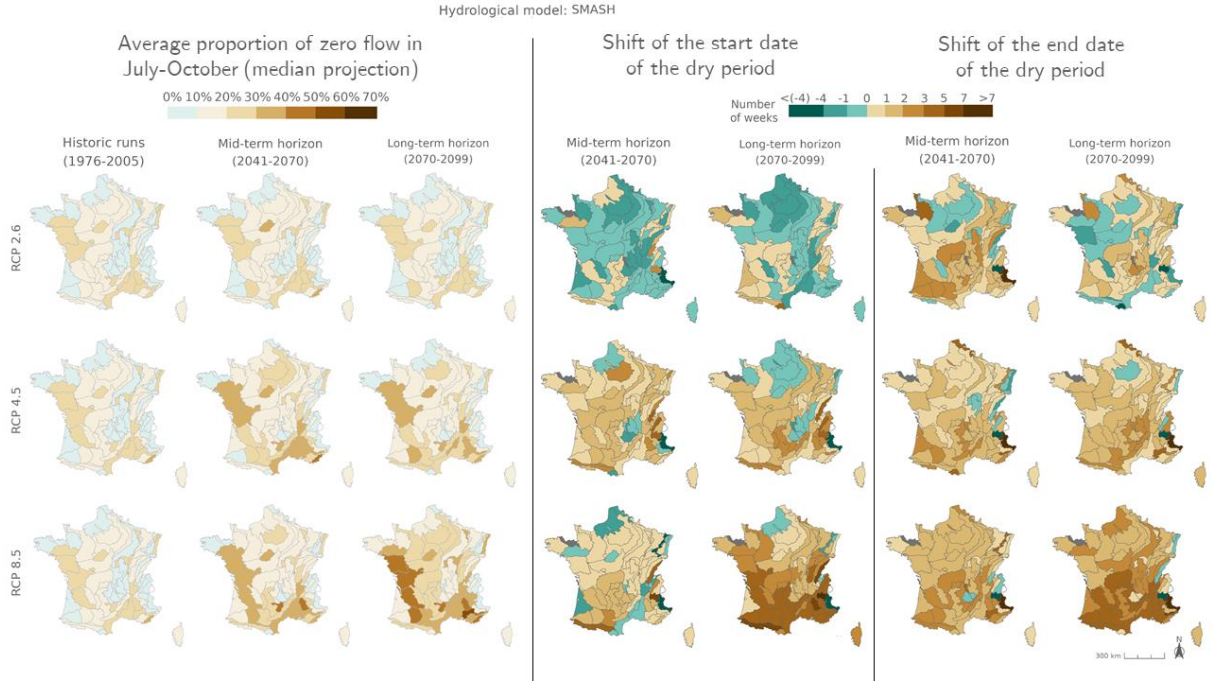

Figure H4: Ensemble median of changes in mPFI7-10 (columns 1 to 3), and ensemble median shift of the start date Ts (columns 4 and 5) and the end date Te (columns 6 and 7) of the dry period over the two periods H1 and H2 under the three RCPs for the SMASH hydrological model, relative to the baseline period H0. The shift, expressed in week, takes one positive value when the duration of the dry period increases.

https://doi.org/10.5194/egusphere-2024-2737
Preprint. Discussion started: 19 September 2024

Narratives

The following figures present time series of the evolution of PFI dynamics at different horizons and under different RCP scenarios for each hydrological model in HER2 12, 57, 81 and 105. Four contrasting scenarios were highlighted among the Explore2 climate projections to illustrate a diversity of potential changes under RCP 8.5. These story lines range from "Strong warming and strong summer (and annual) drying", selected as one of the most extreme climate projections, to “Moderate warming and precipitation change” with less pronounced alterations, with two alternative projections named “Dry all year, reduced winter recharge” and “Hot and humid all seasons”. They are also illustrated here to present distinct hydrological nuances.

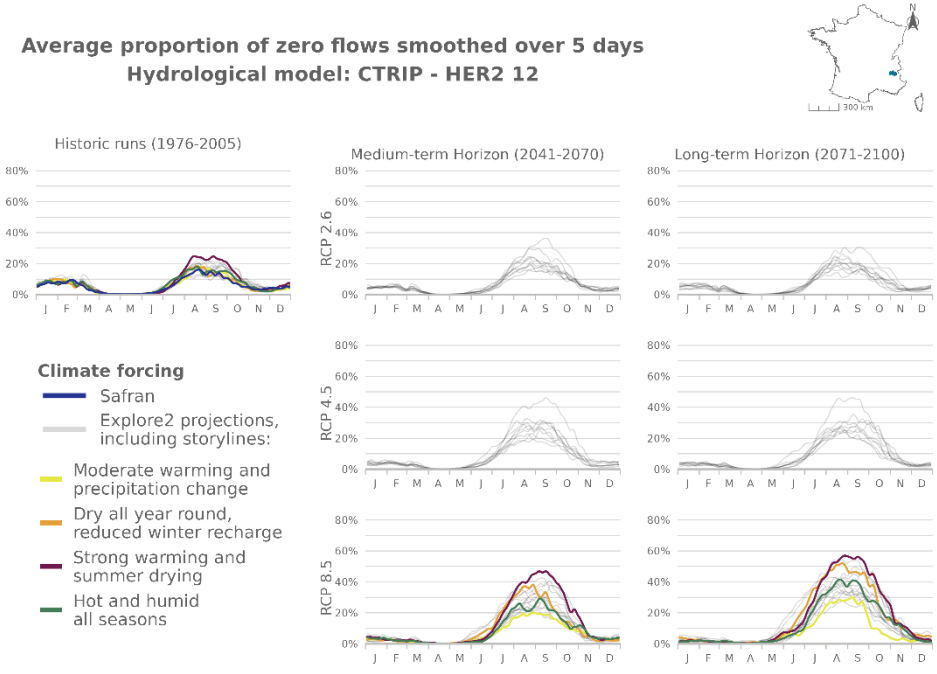

Figure H5: Time series of the evolution of PFI dynamics at different horizons under different RCP scenarios for CTRIP hydrological models in HER 12

https://doi.org/10.5194/egusphere-2024-2737
Preprint. Discussion started: 19 September 2024

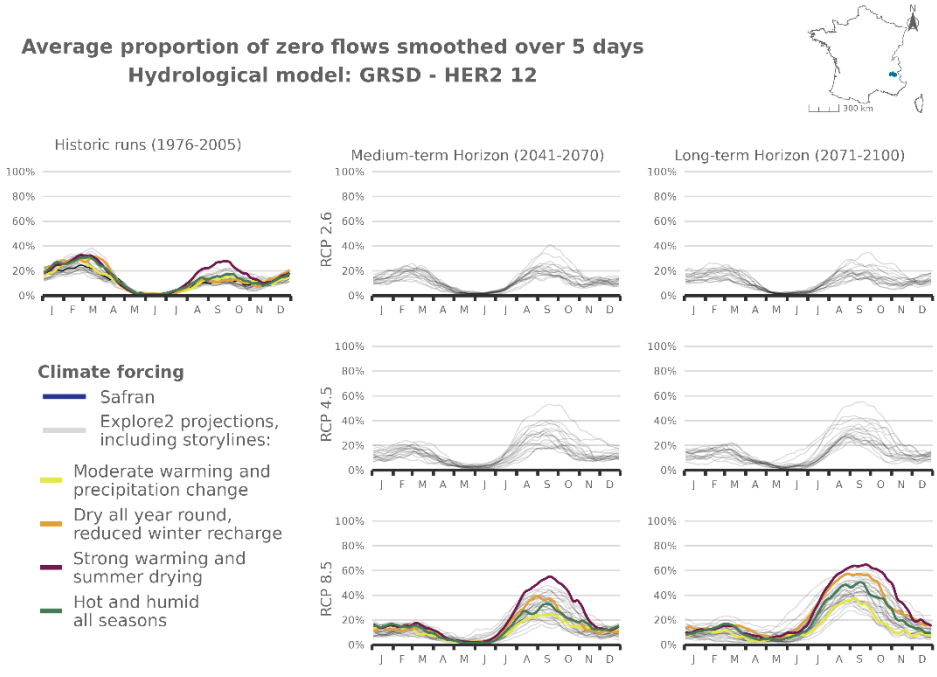

Figure H6: Time series of the evolution of PFI dynamics at different horizons under different RCP scenarios for GRSD hydrological models in HER 12

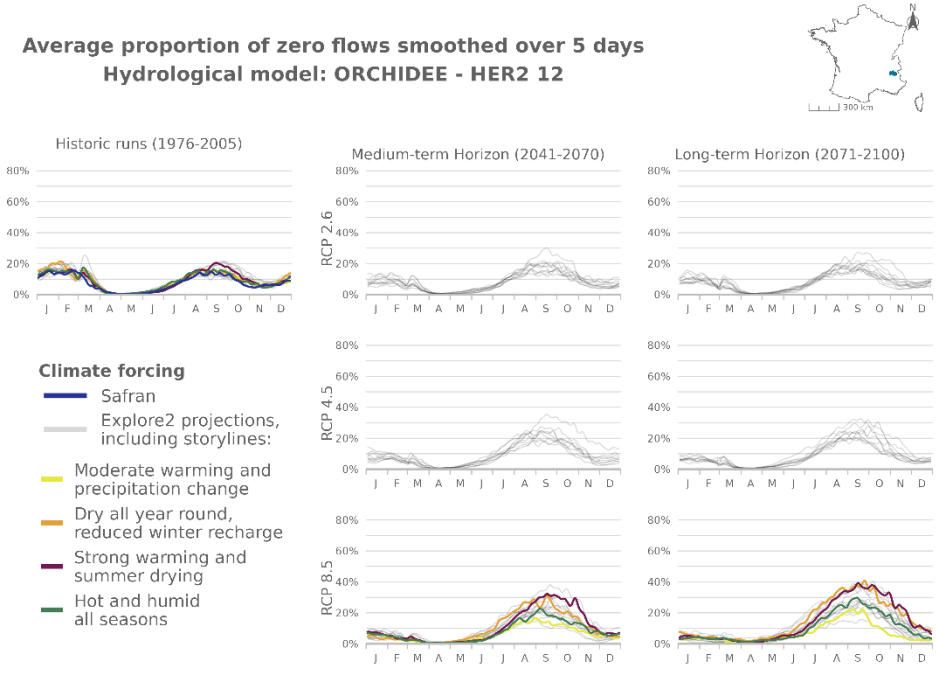

Figure H7: Time series of the evolution of PFI dynamics at different horizons under different RCP scenarios for ORCHIDEE hydrological models in HER 12

https://doi.org/10.5194/egusphere-2024-2737
Preprint. Discussion started: 19 September 2024

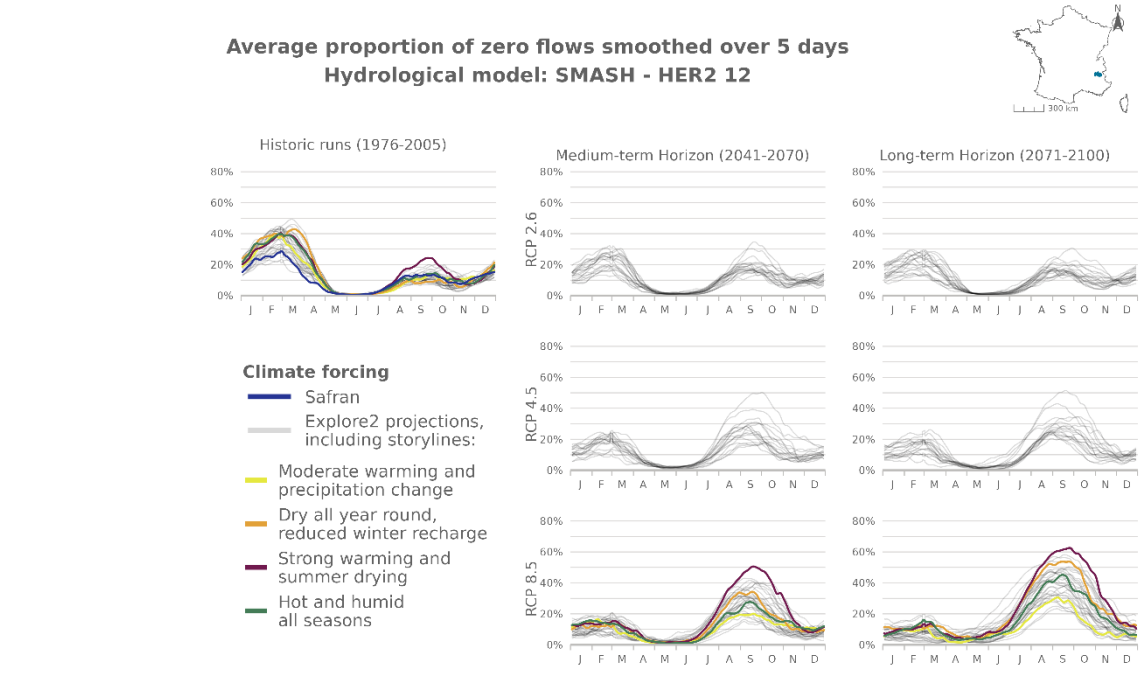

Figure H8: Time series of the evolution of PFI dynamics at different horizons under different RCP scenarios for SMASH hydrological models in HER 12

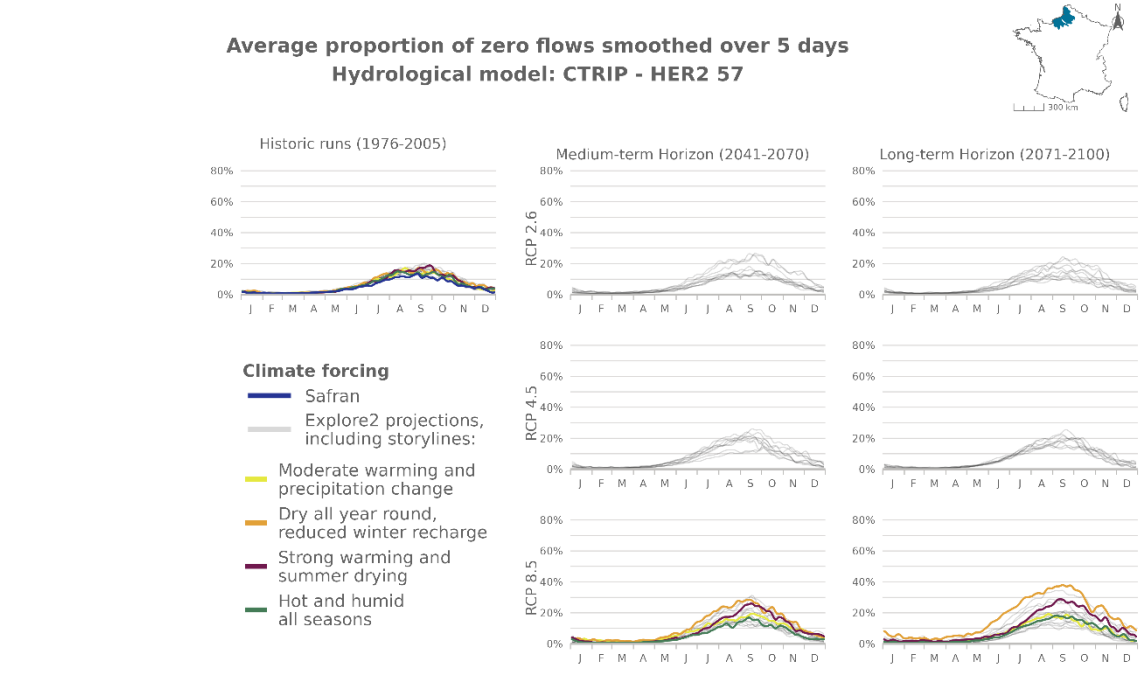

Figure H9: Time series of the evolution of PFI dynamics at different horizons under different RCP scenarios for CTRIP hydrological models in HER 57

https://doi.org/10.5194/egusphere-2024-2737
Preprint. Discussion started: 19 September 2024

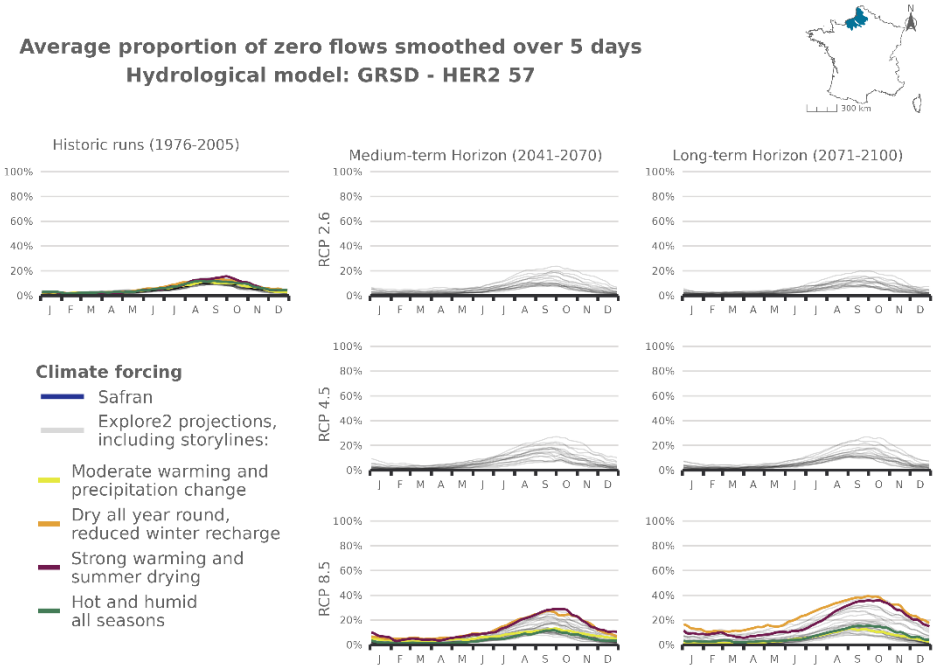

Figure H10: Time series of the evolution of PFI dynamics at different horizons under different RCP scenarios for GRSD hydrological models in HER 57

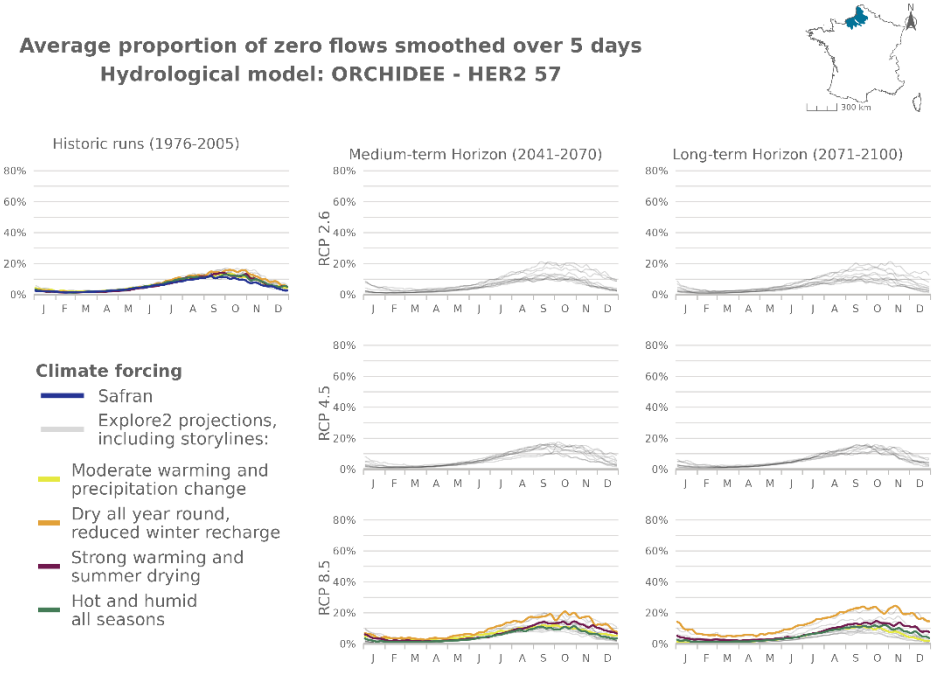

Figure H11: Time series of the evolution of PFI dynamics at different horizons under different RCP scenarios for ORCHIDEE hydrological models in HER 57

https://doi.org/10.5194/egusphere-2024-2737
Preprint. Discussion started: 19 September 2024

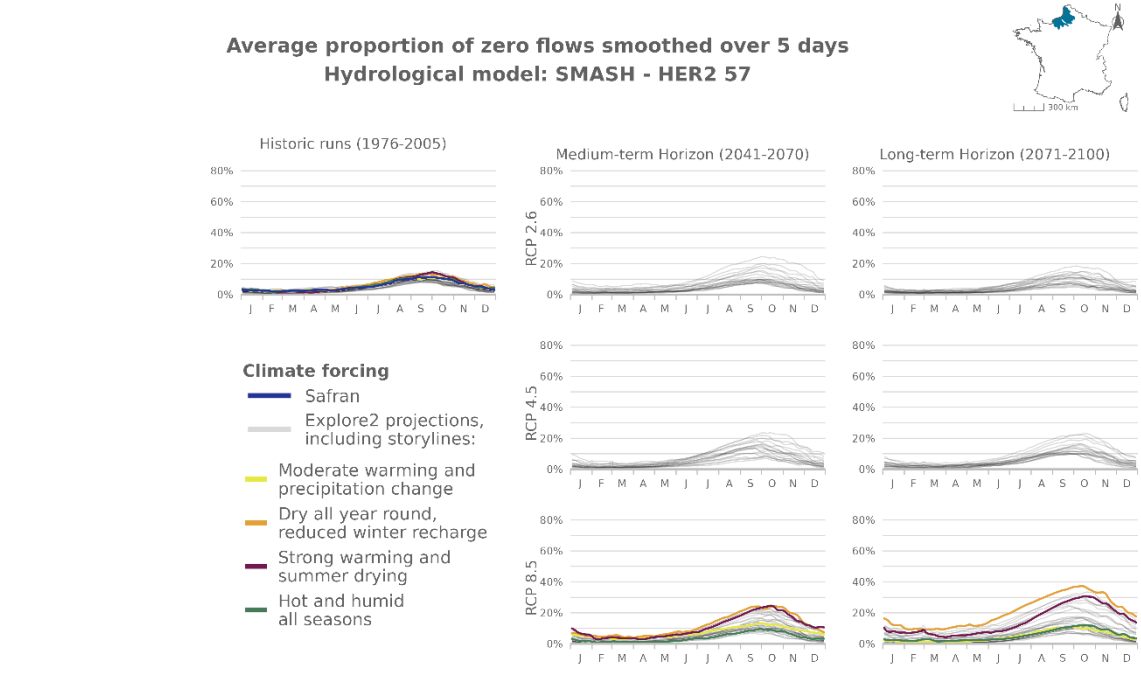

Figure H12: Time series of the evolution of PFI dynamics at different horizons under different RCP scenarios for SMASH hydrological models in HER 57

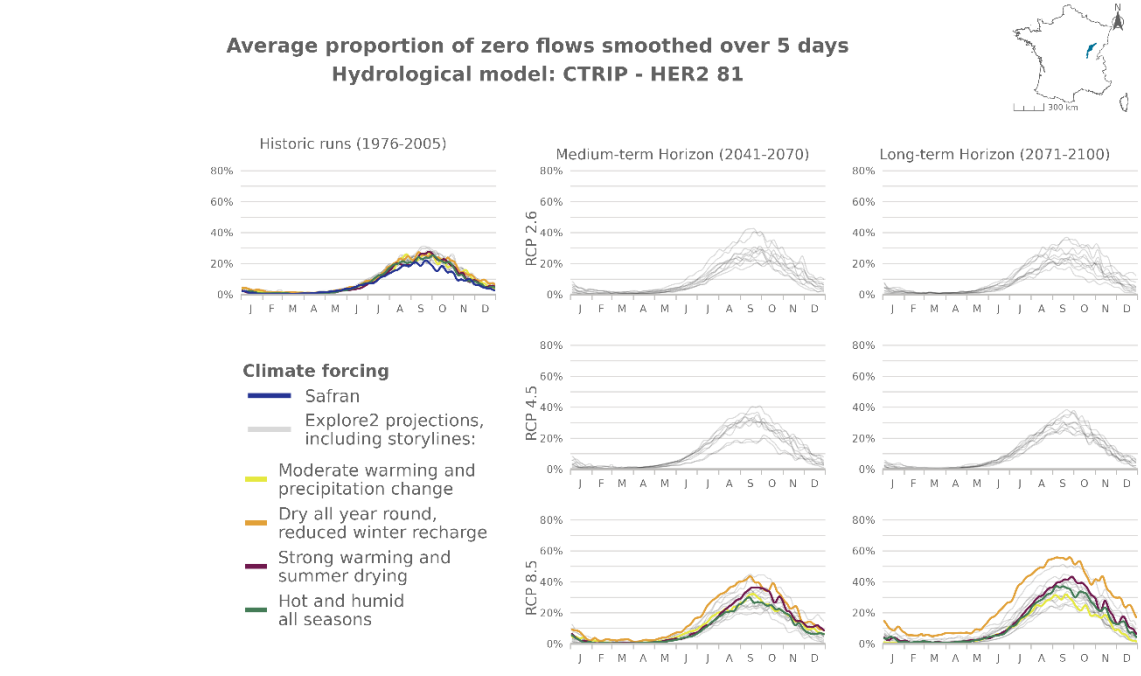

Figure H13: Time series of the evolution of PFI dynamics at different horizons under different RCP scenarios for CTRIP hydrological models in HER 81

https://doi.org/10.5194/egusphere-2024-2737
Preprint. Discussion started: 19 September 2024

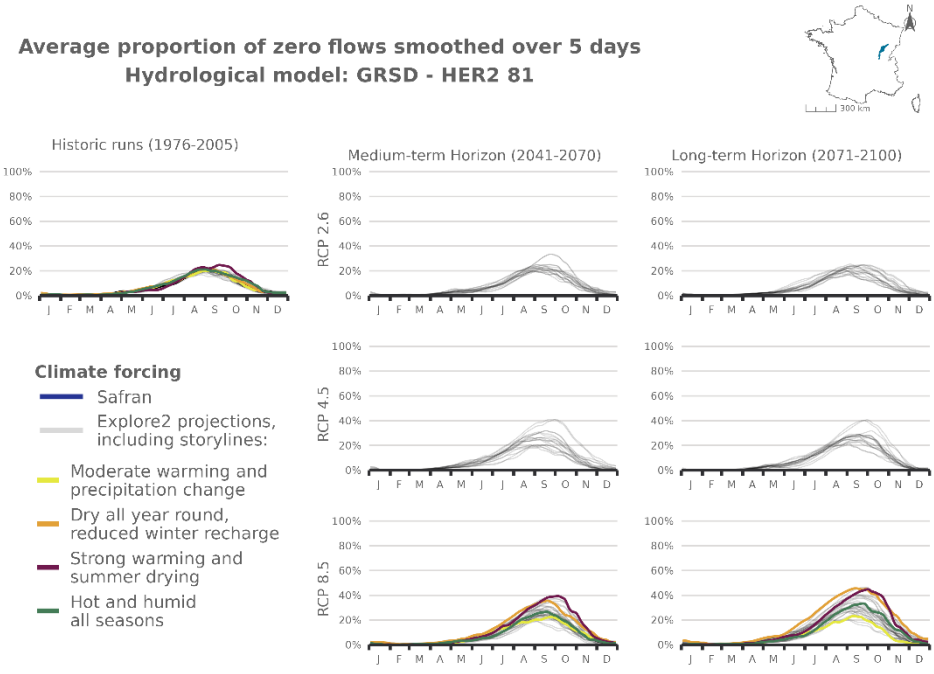

Figure H14: Time series of the evolution of PFI dynamics at different horizons under different RCP scenarios for GRSD hydrological models in HER 81

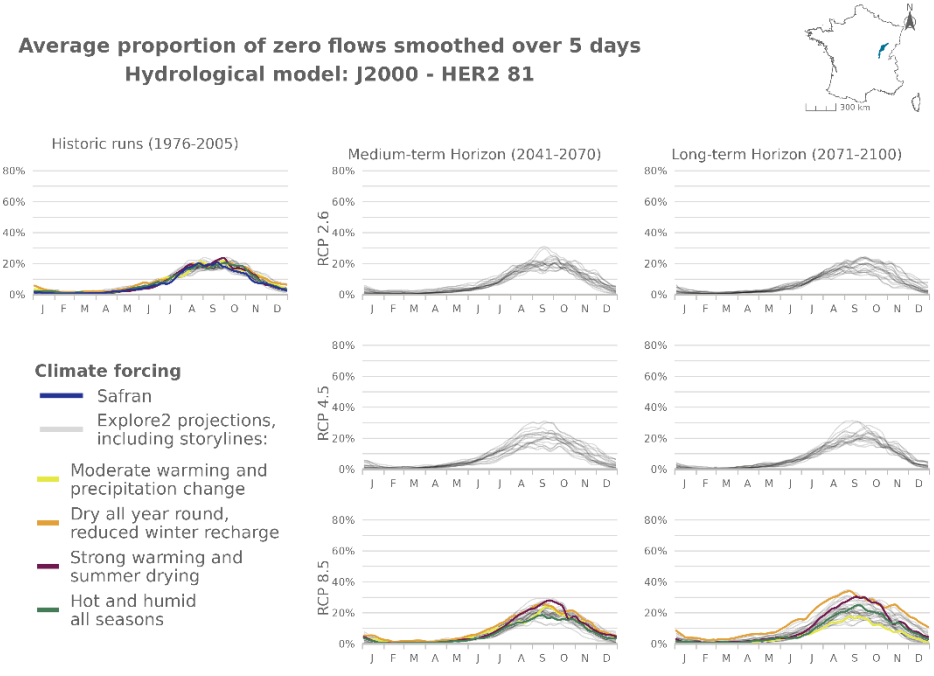

Figure H15: Time series of the evolution of PFI dynamics at different horizons under different RCP scenarios for J2000 hydrological models in HER 81

https://doi.org/10.5194/egusphere-2024-2737
Preprint. Discussion started: 19 September 2024

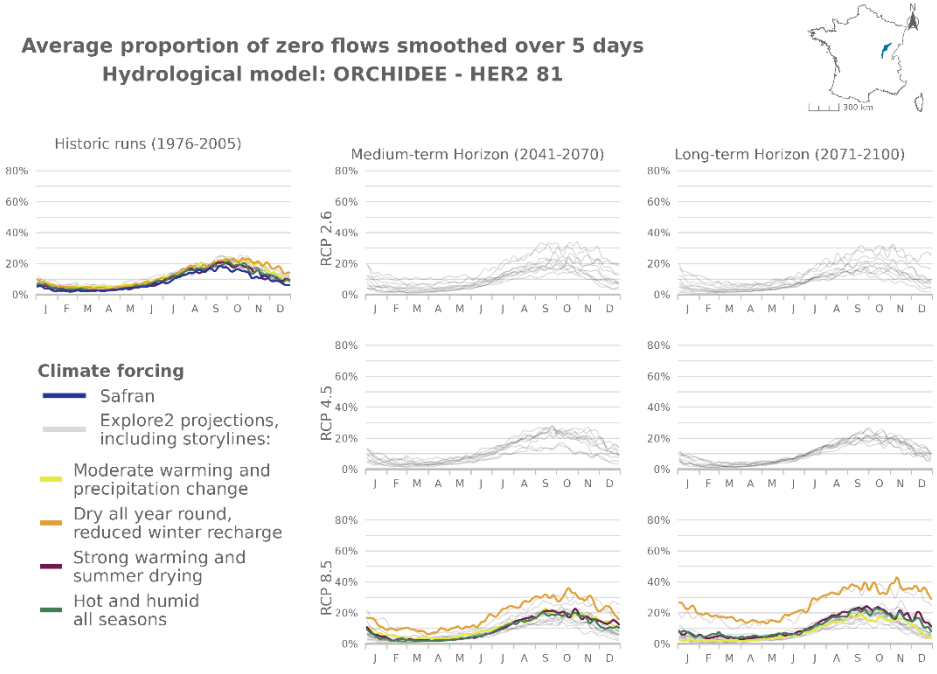

Figure H16: Time series of the evolution of PFI dynamics at different horizons under different RCP scenarios for ORCHIDEE hydrological models in HER 81

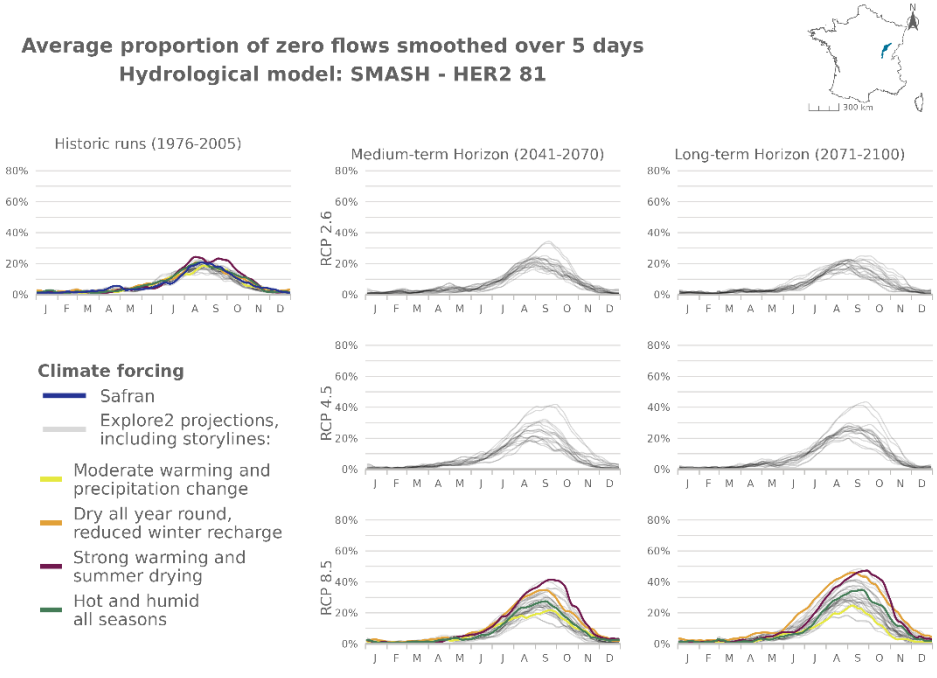

Figure H17: Time series of the evolution of PFI dynamics at different horizons under different RCP scenarios for SMASH hydrological models in HER 81

https://doi.org/10.5194/egusphere-2024-2737
Preprint. Discussion started: 19 September 2024

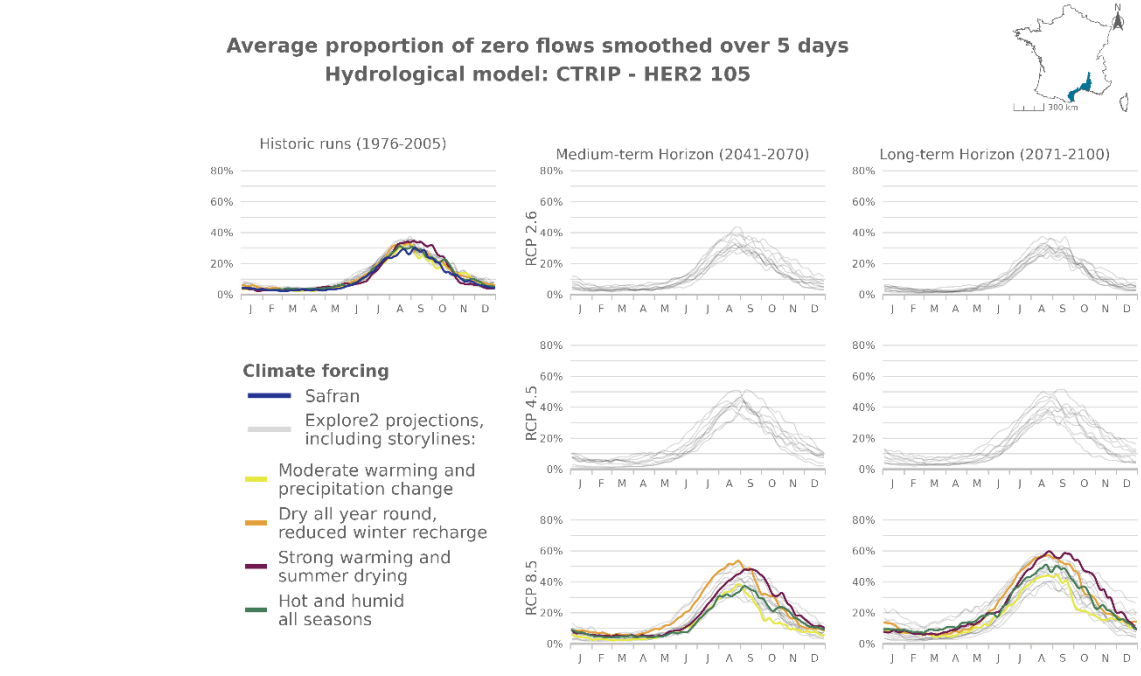

Figure H18: Time series of the evolution of PFI dynamics at different horizons under different RCP scenarios for CTRIP hydrological models in HER 105

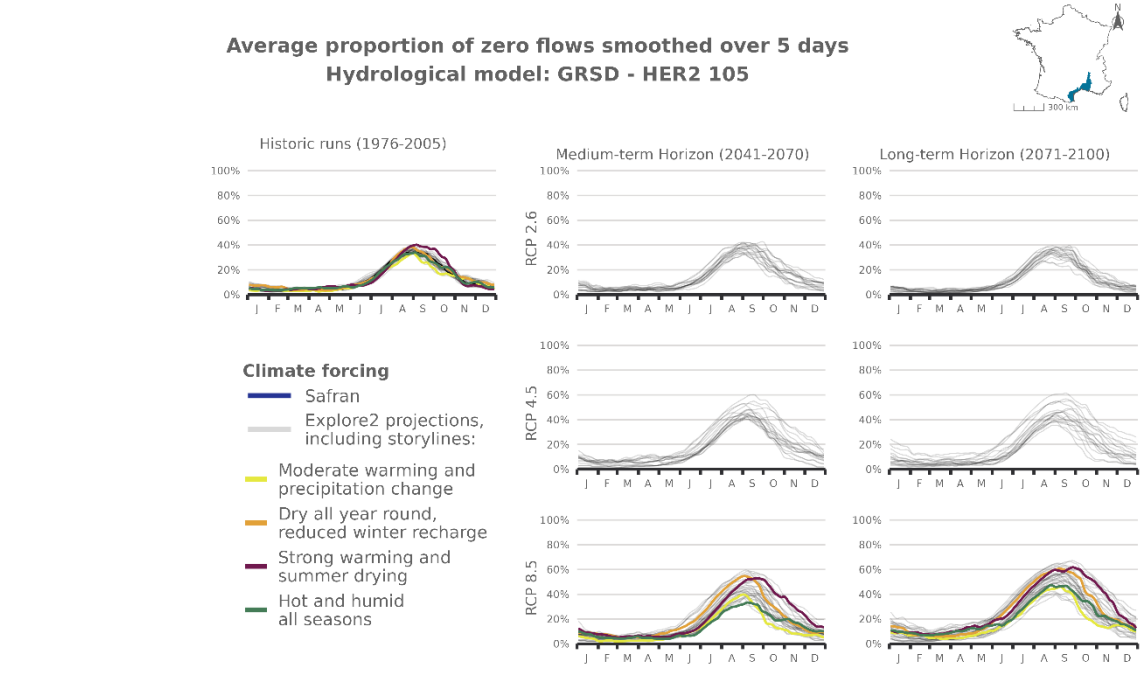

Figure H19: Time series of the evolution of PFI dynamics at different horizons under different RCP scenarios for GRSD hydrological models in HER 105

https://doi.org/10.5194/egusphere-2024-2737
Preprint. Discussion started: 19 September 2024

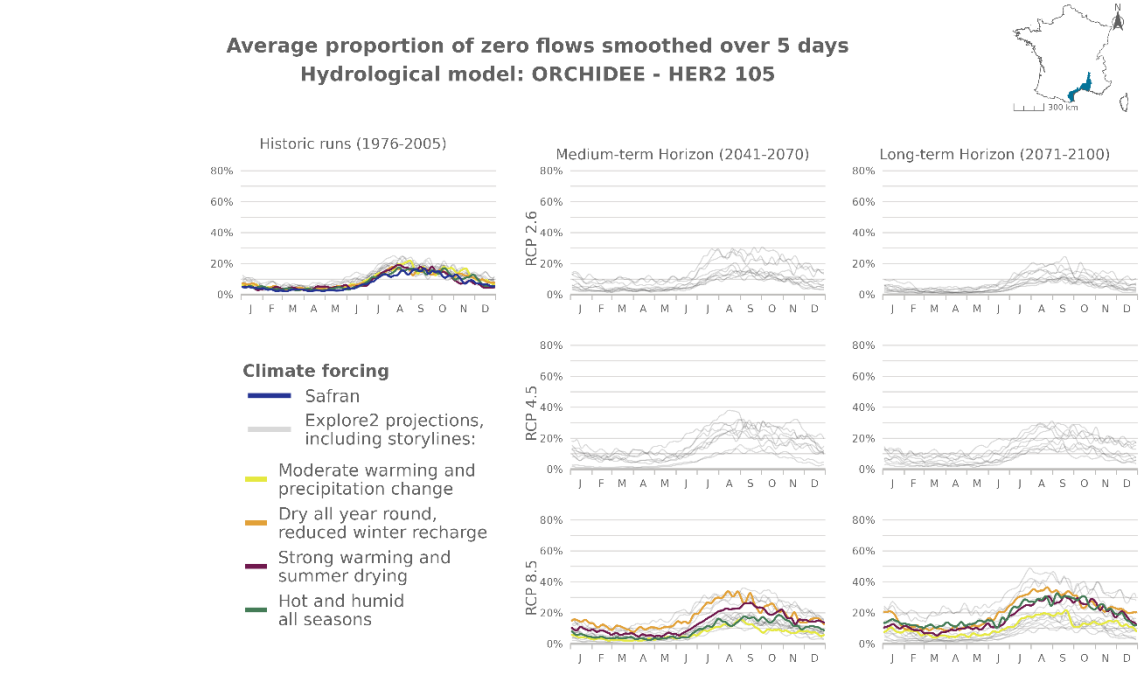

Figure H20: Time series of the evolution of PFI dynamics at different horizons under different RCP scenarios for ORCHIDEE hydrological models in HER 105

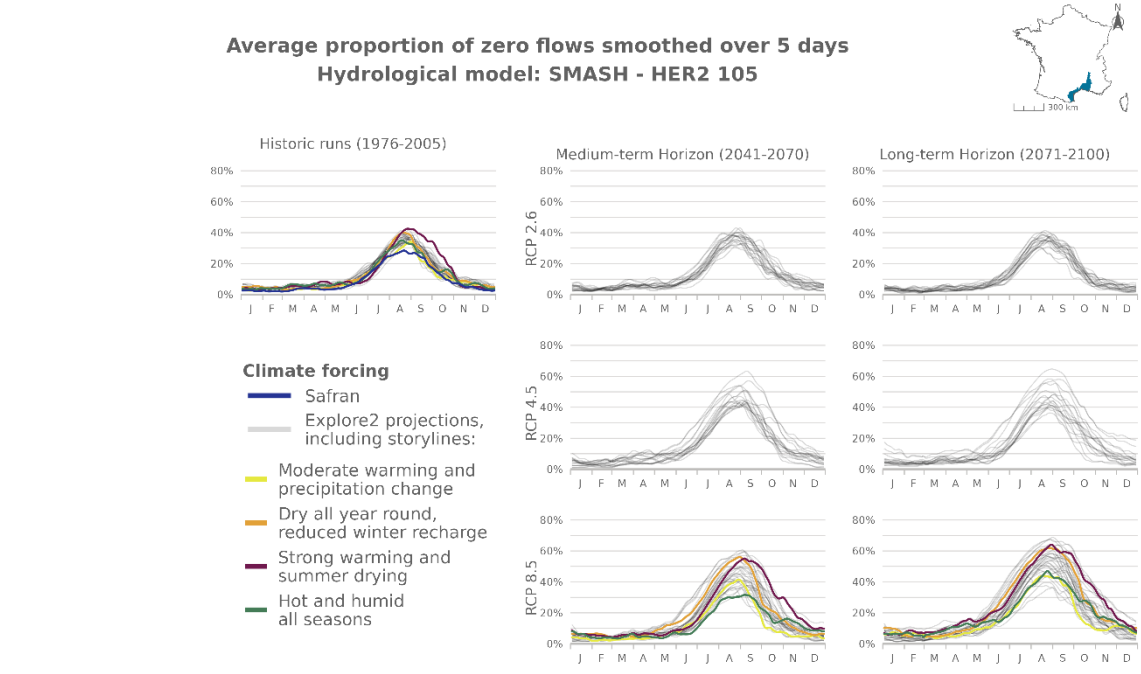

Figure H21: Time series of the evolution of PFI dynamics at different horizons under different RCP scenarios for SMASH hydrological models in HER 105

https://doi.org/10.5194/egusphere-2024-2737
Preprint. Discussion started: 19 September 2024

Appendix I: Agreement between changes under RCP 4.5

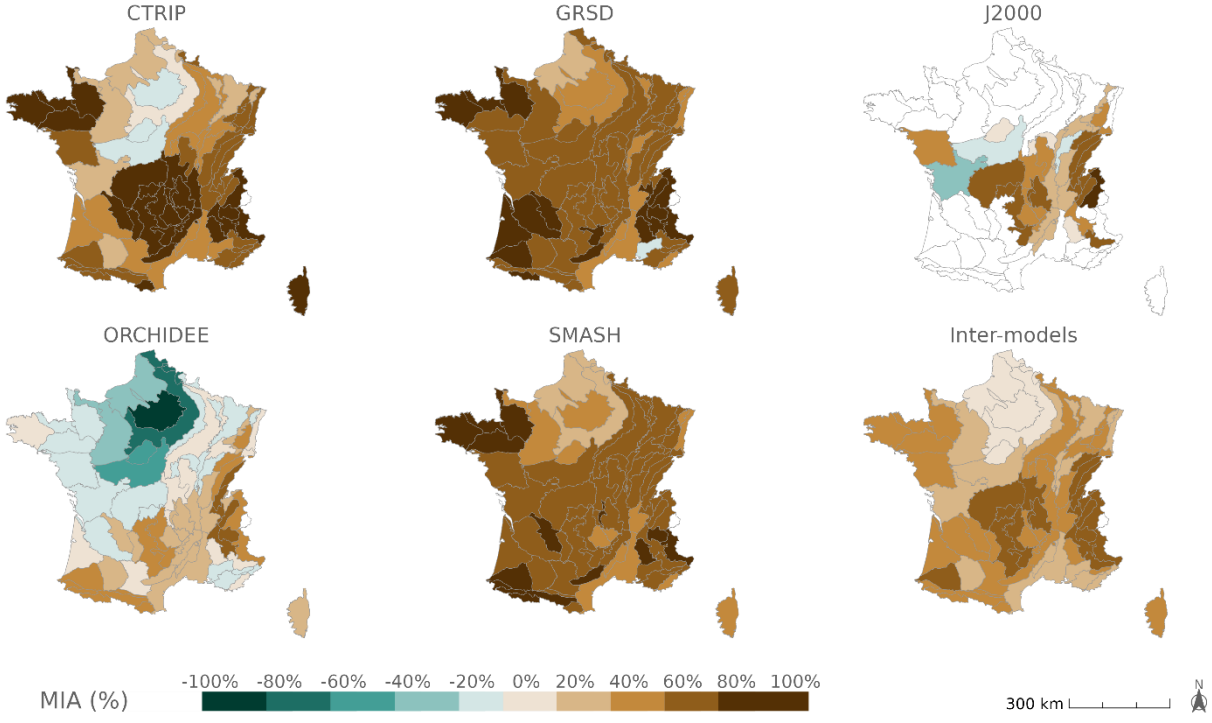

Figure I1: Agreement between projections of mPFI7-10 for each hydrological model and inter-model agreement on the change signal of mPFI7-10 under the RCP 4.5 scenario.

Code availability

The codes are available at https://github.com/tjaouen/PostDocINRAE

Data availability

The Explore2 streamflow projections are available at https://entrepot.recherche.data.gouv.fr/dataverse/explore2 and are described in detail by Sauquet et al., in prep.

Author contribution

Dr. Tristan Jaouen, Dr. Lionel Benoit and Dr. Eric Sauquet designed the experiments and Dr. Tristan Jaouen carried them out. Louis Héraut organized the data from the Explore2 project and made it available. Dr. Tristan Jaouen and Dr. Eric Sauquet

developed the model code. Dr. Tristan Jaouen performed the simulations. Dr. Tristan Jaouen prepared the manuscript with contributions from all co-authors.

Competing interests

The authors declare that they have no conflict of interest.

References

Acuña, V., Datry, T., Marshall, J., Barceló, D., Dahm, C. N., Ginebreda, A., McGregor, G., Sabater, S., Tockner, K., and Palmer, M. A.: Why should we care about temporary waterways?, Science, 343, 1080-1081, https://doi.org/10.1126/science.1246666, 2014.

Aitken, G., Beevers, L., Parry, S., and Facer-Childs, K.: Partitioning model uncertainty in multi-model ensemble river flow projections, Climatic Change, 176, 153, https://doi.org/10.1007/s10584-023-03621-1, 2023.

Barrow, C. J.: World atlas of desertification (United Nations Environment Programme), edited by N. Middleton and D. S. G. Thomas. Edward Arnold, London, 1992. isbn 0 340 55512 2, £89.50 (hardback), ix + 69 pp., Land Degrad. Dev., 3, 249-249, https://doi.org/10.1002/ldr.3400030407, 1992.

Beaufort, A., Lamouroux, N., Pella, H., Datry, T., and Sauquet, E.: Extrapolating regional probability of drying of headwater streams using discrete observations and gauging networks, Hydrol. Earth Syst. Sci., 22, 3033–3051, https://doi.org/10.5194/hess-22-3033-2018, 2018.

Carlson, S. M., Ruhí, A., Bogan, M. T., Hazard, C. W., Ayers, J., Grantham, T. E., Batalla, R. J., and Garcia, C.: Losing flow in free-flowing Mediterranean-climate streams, Front Ecol Environ., 22, e2737, https://doi.org/10.1002/fee.2737, 2024.

Clarke, A., Mac Nally, R., Bond, N., and Lake, P. S.: Macroinvertebrate diversity in headwater streams: a review, Freshwater Biology, 53, 1707-1721, https://doi.org/10.1111/j.1365-2427.2008.02041.x, 2008.

Dai, Z., Amatya, D. M., Sun, G., Trettin, C. C., Li, C., and Li, H.: Climate variability and its impact on forest hydrology on south Carolina coastal plain, USA, Atmosphere. 2011, 2, 330-357, https://doi.org/10.3390/atmos2030330, 2011.

https://doi.org/10.5194/egusphere-2024-2737
Preprint. Discussion started: 19 September 2024

Dakhlaoui, H., Ruelland, D., Tramblay, Y., and Bargaoui, Z.: Evaluating the robustness of conceptual rainfall-runoff models under climate variability in northern Tunisia, Journal of Hydrology, 550, 201-217, https://doi.org/10.1016/j.jhydrol.2017.04.032, 2017.

De Girolamo, A. M., Barca, E., Leone, M., and Lo Porto, A.: Impact of long-term climate change on flow regime in a Mediterranean basin, Journal of Hydrology: Regional Studies, 41, 101061. https://doi.org/10.1016/j.ejrh.2022.101061, 2022.

De Lavenne, A., Thirel, G., Andréassian, V., Perrin, C., and Ramos, M.-H.: Spatial variability of the parameters of a semi-distributed hydrological model, Proc. IAHS, 373, 87–94, https://doi.org/10.5194/piahs-373-87-2016, 2016.

Decharme, B., Delire, C., Minvielle, M., Colin, J., Vergnes, J.-P., Alias, A., et al.: Recent changes in the ISBA-CTRIP land surface system for use in the CNRM-CM6 climate model and in global off-line hydrological applications, Journal of Advances in Modelling Earth Systems, 11, 1207–1252, https://doi.org/10.1029/2018MS001545, 2019.

Delso, J., Magdaleno, F., and Fernández-Yuste, J. A.: Flow patterns in temporary rivers: a methodological approach applied to southern Iberia, Hydrological Sciences Journal, 62, 1551-1563, https://doi.org/10.1080/02626667.2017.1346375, 2017.

Dhungel, S., Tarboton, D. G., Jin, J., and Hawkins, C. P.: Potential effects of climate change on ecologically relevant streamflow regimes, River Res. Applic., 32, 1827-1840, https://doi.org/10.1002/rra.3029, 2016.

Döll, P., Hasan, H. M. M., Schulze, K., Gerdener, H., Börger, L., Shadkam, S., Ackermann, S., Hosseini-Moghari, S.-M., Müller Schmied, H., Güntner, A., and Kusche, J.: Leveraging multi-variable observations to reduce and quantify the output uncertainty of a global hydrological model: evaluation of three ensemble-based approaches for the Mississippi River basin, Hydrol. Earth Syst. Sci., 28, 2259-2295, https://doi.org/10.5194/hess-28-2259-2024, 2024.

Döll, P., and Schmied, H. M.: How is the impact of climate change on river flow regimes related to the impact on mean annual runoff? A global-scale analysis, Environ. Res. Lett., 7, 14037-11, https://doi.org/10.1088/1748-9326/7/1/014037, 2012.

Döll, P., and Zhang, J.: Impact of climate change on freshwater ecosystems: a global-scale analysis of ecologically relevant river flow alterations, Hydrol. Earth Syst. Sci., 14, 783–799, https://doi.org/10.5194/hess-14-783-2010, 2010.

Evin, G., Hingray, B., Blanchet, J., Eckert, N., Morin, S., and Verfaillie, D.: Partitioning uncertainty components of an incomplete ensemble of climate projections using data augmentation, Journal of Climate, 32, 2423-2440, https://doi.org/10.1175/jcli-d-18-0606.1, 2019.

Evin, G., Hingray, B., Ducharne, A., and Sauquet, E.: Ensemble de projections Explore2 : Changements moyens et incertitudes associées, INRAE - IGE; CNRS - IGE; CNRS - IPSL; INRAE, https://hal.science/hal-04609542, 2024.

Evin, G., Somot, S., and Hingray, B.: Balanced estimate and uncertainty assessment of European climate change using the large EURO-CORDEX regional climate model ensemble, Earth System Dynamics, 12, 1543-1569, https://doi.org/10.5194/esd-12-1543-2021, 2021.

Finn, D., Bonada, N., Múrria, C., and Hughes, J.: Small but mighty: headwaters are vital to stream network biodiversity at two levels of organization, Journal of the North American Benthological Society, 30, 963-980, https://doi.org/10.1899/11-012.1, 2011.

Gallart, F., Prat, N., García-Roger, E. M., Latron, J., Rieradevall, M., Llorens, P., Barberá, G. G., Brito, D., De Girolamo, A. M., Lo Porto, A., Buffagni, A., Erba, S., Neves, R., Nikolaidis, N. P., Perrin, J. L., Querner, E. P., Quiñonero, J. M., Tournoud, M. G., Tzoraki, O., Skoulikidis, N., Gómez, R., Sánchez-Montoya, M. M., and Froebrich, J.: A novel approach to analysing the regimes of temporary streams in relation to their controls on the composition and structure of aquatic biota, Hydrol. Earth Syst. Sci., 16, 3165–3182, https://doi.org/10.5194/hess-16-3165-2012, 2012.

Geris, J., Tetzlaff, D., and Soulsby, C.: Resistance and resilience to droughts: Hydropedological controls on catchment storage and run-off response, Hydrological Processes, 29, 4579-4593, https://doi.org/10.1002/hyp.10480, 2015.

Gupta, H., Kling, H., Yilmaz, K., and Martinez, G.: Decomposition of the mean squared error and NSE performance criteria: Implications for improving hydrological modelling, Journal of Hydrology, 377, 80-91, https://doi.org/10.1016/j.jhydrol.2009.08.003, 2009.

Halloran, L., Millwater, J., Hunkeler, D., and Arnoux, M.: Climate change impacts on groundwater discharge-dependent streamflow in an alpine headwater catchment, Science of The Total Environment, 902, 166009. https://doi.org/10.1016/j.scitotenv.2023.166009, 2023.

Huang, P., Ducharne, A., Rinchiuso, L., Polcher, J., Baratgin, L., Bastrikov, V., and Sauquet, E.: Multi-objective calibration and evaluation of the ORCHIDEE land surface model over France at high resolution, EGUsphere [preprint], https://doi.org/10.5194/egusphere-2024-445, 2024.

Jaeger, K. L., Olden, J. D., and Pelland, N. A.: Climate change poised to threaten hydrologic connectivity and endemic fishes in dryland streams, Proceedings of the National Academy of Sciences of the United States of America, 111, 13894-13899, https://doi.org/10.1073/pnas.1320890111, 2014.

Jay-Allemand, M., Javelle, P., Gejadze, I., Arnaud, P., Malaterre, P.-O., Fine, J.-A., and Organde, D.: On the potential of variational calibration for a fully distributed hydrological model: application on a Mediterranean catchment, Hydrol. Earth Syst. Sci., 24, 5519–5538, https://doi.org/10.5194/hess-24-5519-2020, 2020.

Leigh, C., and Datry, T.: Drying as a primary hydrological determinant of biodiversity in river systems: A broad-scale analysis, Ecography. 40, 487-499, https://doi.org/10.1111/ecog.02230, 2017.

Leleu, I., Tonnelier, I., Puechberty, R., Gouin, P., Viquendi, I., Cobos, L., Foray, A., Baillon, M., and Ndima, P.-O.: Re-founding the national information system designed to manage and give access to hydrometric data, La Houille Blanche, 100, 25-32, https://doi.org/10.1051/lhb/2014004, 2014.

Meyer, J., Strayer, D., Wallace, J., Eggert, S., Helfman, G., and Leonard, N.: The contribution of headwater streams to biodiversity in river networks, JAWRA Journal of the American Water Resources Association, 43, 86-103, https://doi.org/10.1111/j.1752-1688.2007.00008.x, 2007.

Morel, M., Pella, H., Branger, F., Sauquet, E., Grenouillet, G., Côte, J., Braud, I., and Lamouroux, N.: Catchment-scale applications of hydraulic habitat models: Climate change effects on fish, Ecohydrology, 16, e2513, https://doi.org/10.1002/eco.2513, 2023.

Nash, J. E., and Sutcliffe, J. V.: River flow forecasting through conceptual models part I-A discussion of principles, Journal of Hydrology, 10, 282-290, http://dx.doi.org/10.1016/0022-1694(70)90255-6, 1970.

Nowak C., and Durozoi B.: Guide de dimensionnement et de mise en œuvre du suivi national des étiages estivaux, ONEMA, 33 p., 2012.

Pumo, D., Caracciolo, D., Viola, F., and Noto, L. V.: Climate change effects on the hydrological regime of small non-perennial river basins, Sci Total Environ., 542, 76-92, https://doi.org/10.1016/j.scitotenv.2015.10.109, 2016.

Reidy Liermann, C., Olden, J., Beechie, T., Kennard, M., Skidmore, P., Konrad, C., and Imaki, H.: Hydrogeomorphic classification of Washington State rivers to support emerging environmental flow management strategies, River Research and Applications, 28, 1340-1358, https://doi.org/10.1002/rra.1541, 2012.

Reynolds, L. V., Shafroth, P. B., and Poff, L.: Modeled intermittency risk for small streams in the Upper Colorado River Basin under climate change, Journal of Hydrology, 523, 768-780, https://doi.org/10.1016/j.jhydrol.2015.02.025, 2015.

Rutkowska, A., Osuch, M., Żelazny, M., Banasik, K., and Klimek, M.: Climatic and anthropogenic drivers of zero-flow events in intermittent rivers in Poland, Journal of Water and Land Development, 57, 52-61, https://doi.org/10.24425/jwld.2023.145335, 2023.

Sarremejane, R., Cañedo-Argüelles, M., Prat, N., Mykrä, H., Muotka, T., and Bonada, N.: Do metacommunities vary through time? Intermittent rivers as model systems, Journal of Biogeography, 44, 2752-2763, https://doi.org/10.1111/jbi.13077, 2017.

Sauquet, E., Beaufort, A., Sarremejane, R., and Thirel, G.: Predicting flow intermittence in France under climate change, Hydrological Sciences Journal, 66, 2046-2059, https://doi.org/10.1080/02626667.2021.1963444, 2021.

Scheller, M., Van Meerveld, I., and Seibert, J.: How well can people observe the flow state of temporary streams?, Frontiers in Environmental Science, 12, https://doi.org/10.3389/fenvs.2024.1352697, 2024.

Schneider, C., Laizé, C. L. R., Acreman, M. C., and Flörke, M.: How will climate change modify river flow regimes in Europe?, Hydrol. Earth Syst. Sci., 17, 325–339, https://doi.org/10.5194/hess-17-325-2013, 2013.

Sefton, C. E.M., Parry, S., England, J., and Angell, G.: Visualising and quantifying the variability of hydrological state in intermittent rivers, Fundamental and Applied Limnology [in special issue: The ecohydrology of temporary streams], 193, 21-38, https://doi.org/10.1127/fal/2019/1149, 2019.

Strohmenger, L., Sauquet, E., Bernard, C., Bonneau, J., Branger, F., Bresson, A., Brigode, P., Buzier, R., Delaigue, O., Devers, A., Evin, G., Fournier, M., Hsu, S.-C., Lanini, S., De Lavenne, A., Lemaitre-Basset, T., Magand, C., Mendoza Guimarães, G., Mentha, M., Munier, S., Perrin, C., Podechard, T., Rouchy, L., Sadki, M., Soutif-Bellenger, M., Tilmant, F., Tramblay, Y., Véron, A.-L., Vidal, J.-P., and Thirel, G.: On the visual detection of non-natural records in streamflow time series: challenges and impacts, Hydrol. Earth Syst. Sci., 27, 3375–3391, https://doi.org/10.5194/hess-27-3375-2023, 2023.

https://doi.org/10.5194/egusphere-2024-2737
Preprint. Discussion started: 19 September 2024

Tramblay, Y., Rutkowska, A., Sauquet, E., Sefton, C., Laaha, G., Osuch, M., Albuquerque, M. T. D., Alves, M., Banasik, K., Beaufort, A., et al.: Trends in flow intermittence for European rivers, Hydrological Sciences Journal, 66, 37-49, https://doi.org/10.1080/02626667.2020.1849708, 2020.

Tramblay, Y., and Somot, S.: Future evolution of extreme precipitation in the Mediterranean, Climatic Change, 151, 289-302, https://doi.org/10.1007/s10584-018-2300-5, 2018.

Van Meerveld, H. J. I., Sauquet, E., Gallart, F., Sefton, C., Seibert, J., and Bishop, K.: Aqua temporaria incognita, Hydrological Processes, 34, 5704–5711, https://doi.org/10.1002/hyp.13979, 2020.

Verfaillie, D., Lafaysse, M., Déqué, M., Eckert, N., Lejeune, Y., and Morin, S.: Multi-component ensembles of future meteorological and natural snow conditions for 1500 m altitude in the Chartreuse mountain range, Northern French Alps, The Cryosphere, 12, 1249–1271, https://doi.org/10.5194/tc-12-1249-2018, 2018.

Vicente-Serrano, M. S., McVicar, T. R., Miralles, D. G., Yang, Y., and Tomas-Burguera, M.: Unravelling the influence of atmospheric evaporative demand on drought and its response to climate change, WIREs Clim Change, 11, e632, https://doi.org/10.1002/wcc.632, 2020.

Vidal, J.-P., Martin, E., Franchistéguy, L., Baillon, M. and Soubeyroux, J.-M.: A 50-year high-resolution atmospheric reanalysis over France with the Safran system, Int. J. Climatol., 30, 1627-1644, https://doi.org/10.1002/joc.2003, 2010.

Wasson, J. G., Chandesris, A., Pella, H., and Blanc, L.: Définition des hydro-écorégions françaises métropolitaines. Approche régionale de la typologie des eaux courantes et éléments pour la définition des peuplements de référence d'invertébrés, Irstea, pp.190, hal-02580774, 2002.

Zipper, S., Hammond, J., Shanafield, M., Zimmer, M., Datry, T., Jones, C., Kaiser, K., Godsey, S., Burrows, R., and Blaszczak, J., et al.: Pervasive changes in stream intermittency across the United States, Environmental Research Letters, 16, 084033, https://doi.org/10.1088/1748-9326/ac14ec, 2021.